Sedimentary Geology 395 (2020) 105549

Contents lists available at ScienceDirect

Sedimentary Geology

journal homepage: www.elsevier.com/locate/sedgeo

Dolomitization of shallow-water, mixed siliciclastic-carbonate sequences: The Lower Triassic ramp succession of the Transdanubian Range, Hungary

Orsolya Győri [a,*], János Haas [b], Kinga Hips [a], Georgina Lukoczki [c], Tamás Budai [d], Attila Demény [e], Emese Szőcs [a]

[a] MTA-ELTE Geological, Geophysical and Space Science Research Group, Pázmány P. sétány 1/c, Budapest H–1117, Hungary
[b] Department of Physical and Applied Geology, Eötvös Loránd University, Pázmány P. sétány 1/c, Budapest H–1117, Hungary
[c] University of Kentucky, Kentucky Geological Survey, Mining and Mineral Resources Building, Lexington, KY 40506, USA
[d] Department of Geology and Meteorology, University of Pécs, 7624 Ifjúság útja 6, Pécs, Hungary
[e] Institute for Geological and Geochemical Research, Research Centre for Astronomy and Earth Sciences, Hungarian Academy of Sciences, Budaörsi street 45, Budapest H-1112, Hungary

ARTICLE INFO

Article history:
Received 11 July 2019
Received in revised form 28 October 2019
Accepted 29 October 2019
Available online 01 November 2019

Editor: Dr. J. Knight

Keywords:
Mixed ramp deposits
Dolomite
Diagenesis
Early Triassic
Stable isotopes
Ferroan carbonates

ABSTRACT

The Lower Triassic succession of the Transdanubian Range in Hungary comprises limestones, dolomite, marl, sandstones and siltstones, deposited in tidal flat, lagoon and ooid shoal environments on the marginal ramp of the western Neotethys. Seven cores were chosen for petrographic and stable isotope investigations aiming to reconstruct the paragenetic sequence with special regard to the dolomitization and hydrothermal events. Five lithotypes were differentiated: (i) dolomite, (ii) sandy, silty, clayey dolomite, and dolomarl, (iii), dolomitic siltstone and sandstone, (iv) dolomitic limestone, and (v) limestone. In these lithotypes, three types of dolomites are present: non-ferroan replacive, ferroan replacive, and ferroan cement. Fabric retentive and fabric destructive non-ferroan replacive dolomitization are interpreted to have occurred by seepage reflux. Supporting evidence includes the presence gypsum and anhydrite in the Lower Triassic beds. Stable isotope values of the ferroan dolomite ($\delta^{18}O$ of −10.7 to −4.2‰ and $\delta^{13}C$ of −4.8 to 4.7‰) suggest dolomitization by fluids of relatively high temperature. The similar stable isotope values ($\delta^{18}O$ of −9.3 to −5.8‰ and $\delta^{13}C$ of −1.9 to 2.5‰) of the non-ferroan dolomite phase suggest that the reflux dolomite was overprinted by this second dolomitization event. Traces of exotic minerals, such as barite, chalcopyrite, galena and sulphosalts were found as fillings of vugs and fractures in the dolomite-cemented sandstone. The metals could have been sourced from the underlying Permian red sandstone beds. The heterogeneous sediment composition had profound impact on the diagenesis of these sedimentary successions.

1. Introduction

Mixed siliciclastic-carbonate sequences formed in various depositional settings are common worldwide in the records of different geological ages (e.g., Blanchard et al., 2016; Reis and Suss, 2016; Bassant et al., 2017; Chiarella et al., 2017). Research has been focused on these successions in the past decades for several reasons: (i) to define the environmental controls on their formation (Coffey and Read, 2007; Coffey and Sunde, 2014; Bassant et al., 2017; Chiarella et al., 2017), (ii) to reveal how the carbonate factory is affected by and reacts to the siliciclastic sediment input (Coffey and Read, 2007; Caracciolo et al., 2013; Korngreen and Bialik, 2015; Zeller et al., 2015), (iii) and also for exploratory purposes, since they can form major hydrocarbon reservoirs (McNeill et al., 2004; Kleipool et al., 2015). Diagenesis, especially regarding dolomitization processes associated with these mixed strata, is, however, less studied. In the case studies dealing with the carbonate cementation in sandstones, the siliciclastic grains are predominant (e.g., Morad, 1998). In the mixed rocks, on the other hand, the ratio of carbonate grains is significant and such sediment composition might have considerable effects on their diagenetic history (e.g., Morad et al., 2000).

Lower Triassic shallow marine and mixed siliclastic-carbonate strata of the Transdanubian Range, Hungary, are commonly dolomitized and extensively cemented by ferroan carbonates. Furthermore, these successions host a barite-sulphide-sulphosalt ore indication. These strata have been previously studied mainly from stratigraphic and sedimentologic point of view that provides a good basis to focus on the dolomitization of the formations. The dolomitization previously identified in lagoonal sedimentary rocks was classified as early diagenetic, but no detailed investigation has been carried out, so far.

* Corresponding author.
E-mail address: gyoriorsolya@caesar.elte.hu (O. Győri).

https://doi.org/10.1016/j.sedgeo.2019.105549
0037-0738/

Sulphidic ore indications from the Lower Triassic strata are scarcely mentioned in the Hungarian geological literature and exclusively associated with sedimentary processes (Csalagovits and Virágh, 1968; Raincsák, 1975, 1982).

This study focused on the understanding of the different dolomitization and cementation processes, as well as the origin of the barite-sulphide-sulphosalt mineralization hosted by Lower Triassic formations of the Transdanubian Range. Our aim was to provide details on how classical shallow-burial processes, such as reflux dolomitization can be overprinted by *meso* and telogenetic processes and how these differ in the vicinity of siliciclastic interbeds.

2. Geological setting

The Transdanubian Range Unit in the north-western part of Hungary (Fig. 1) is part of the ALCAPA Megaunit derived from the southern shelf of the Neotethys Ocean (Schmid et al., 2008). The Transdanubian Range is a mountaneous domain within the Transdanubian Range Unit that is made up mostly of Lower Paleozoic to Cenozoic formations. During the Late Permian to Paleogene the depositional area was located between the South Alpine and Upper Austroalpine domains (Haas et al., 1995; Csontos and Vörös, 2004) and approached its present-day position during the Late Paleogene to Early Neogene as a result of lateral extrusion and anticlockwise rotation (Kázmér and Kovács, 1985; Csontos et al., 1992; Csontos and Vörös, 2004; Márton and Márton, 1996; Schmid et al., 2008).

2.1. Depositional setting and stratigraphy

The lihofacies characteristics of the Upper Permian to Lower Triassic formations are mostly controlled by the relative sea-level changes and the climatic conditions of the studied region (Broglio Loriga et al., 1990; Budai and Haas, 1997; Haas et al., 2012). The chronostratigraphic assignment and correlation of the formations (Fig. 2) is founded mainly on biostratigraphy of bivalves, foraminifera and paynomorphs (Góczán et al., 1986; Broglio Loriga et al., 1990). In the Late Permian, the Transdanubian Range was part of the coastal belt of the Tethys. In its SW part, alluvial conglomerate, sandstone and siltstone ("continental red beds", Balatonfelvidék Sandstone Fm.) grade into continental and evaporitic (sabkha) deposits (Tabajd Fm.) and lagoonal evaporitic dolomites (Dinnyés Dolomite Fm.) towards the NE. Sea-level rise at the Permian–Triassic boundary led to marine transgression of the former alluvial plain and the establishment of a wide homoclinal ramp in the Early Induan (Haas and Budai, 1995, 1999) (Fig. 2).

The lower (Induan) part of the Lower Triassic succession is made up by three coeval formations (Fig. 2). Their sedimentological features, characteristic fossils and depositional environment are summarized in Table 1. In the NE part of the Transdanubian Range, the Permian lagoonal evaporitic dolomite is overlain by Lower Induan oolitic–bioclastic limestones (Alcsútdoboz Limestone Fm.) deposited on the outer ramp. Southwestward the Permian continental red beds are covered by a dolomitic marl succession of shallow inner ramp (mud-shoal) facies (Arács Marl Fm.). Continentward, mixed rock types consisting dominantly of silty and sandy dolomite with evaporate nodules (Köveskál Dolomite Fm.; Fig. 2) were formed in a restricted lagoon behind the mud-shoals. Characteristic fossils of the Induan formations are microgastropods and bivalve assemblage of low diversity (*Claraia* spp., *Unionites* sp.).

In the Lower Olenekian the appearance of red sandstones and siltstones (Zánka Sandstone Member of the Hidegkút Fm.; Fig. 2) probably record a marked change from dry to wet climate (called the "Campil Event" by Broglio Loriga et al., 1990). Increasing diversity of bivalves (*Unionites* spp., *Neoschizodus* spp., *Pseudomonotis* spp., *Bakevellia*, *Costatoria*, *Eumorphotis*) indicates rising sea-level. Lagoonal to peritidal dolomite (Hidegkút Dolomite Member of the Hidegkút Fm.), locally with anhydrite and/or gypsum, formed in the Middle Olenekian (Haas et al., 1988), suggesting sea-level fall and arid to semi-arid climate (Haas et al., 2012). During the Late Olenekian, silty marl interbedded with carbonate tempestite deposited in a middle to outer ramp setting (Csopak Marl Fm.; Fig. 2). Along with a rich and highly diversed bivalve assemblage it contains ammonites (Tirolites, Dinarites), the first after the P/T boundary mass extinction event. All of these features suggest a sea-level rise, the most significant during the Early Triassic. Since the deposited neritic sediments were not affected by dolomitization it was out of the focus of the current study. The upper part of the Csopak Marl that is rich in crinoidal limestone and sandstone interbeds is gradually overlain by lagoonal dolomite (Aszófő Dolomite Fm. – Lower Anisian), deposited in restricted and evaporitic conditions, reflecting a regressive trend in the latest Olenekian (Broglio Loriga et al., 1990; Budai and Haas, 1997).

2.2. Burial history

The Lower Triassic formations were subjected to progressive burial under younger Triassic mostly shallow marine carbonates (3.0–3.5 km in thickness), and Jurassic to Lower Cretaceous pelagic carbonates (0.5–0.7 km in thickness). The NE–SW trending synform structure of the Transdanubian Range was formed in the late Early Cretaceous compressional regime, induced by the Alpine orogeny (Császár and Haas, 1979; Mindszenty, 1985; Fodor, 1998). Intense denudation took place during the early Late Cretaceous (Turonian–Coniacian) and the Paleocene to earliest Eocene long-lasting subaerial exposure event brought the Triassic formations to the surface in large parts of the Transdanubian Range. The Lower Triassic succession was subject to ~1000 m burial from the Oligocene onwards (Danisik et al., 2015).

3. Samples and Methods

The Lower Triassic formations are exposed by outcrops and scientific exploration wells along the SE and NW limbs of the Transdanubian Range syncline. Seven wells with drill cores were chosen from different parts of the Transdanubian Range for detailed investigation (Fig. 1). The cores are stored in the repository of the Mining and Geological Survey of Hungary.

Different lithologies of the drill cores were sampled and forty-four thin sections were prepared and examined together with approximately 150 thin sections that were made for previous studies (Haas et al., 1988; Broglio Loriga et al., 1990) (their position is indicated on Fig. 3). Terminology for crystal sizes followed Folk (1962). Results of previous X-ray powder diffraction, derivatograph measurements and chemical analysis, available in unpublished reports at the Geological Institute of Hungary, were also used.

A solution of 10% HCl, Alizarin Red-S and potassium ferricyanide (Dickson, 1966) was used to distinguish calcite, dolomite, ferroan calcite, ferroan dolomite (Mg > Fe), ankerite (Fe > Mg) and siderite in the samples. Cathodoluminescence (CL) studies were conducted using a MAAS-Nuclide ELM-3 cold-cathode luminoscope (Measurement and Analysis Systems, Inc., Lowell, MA, US) at the Department of Physical and Applied Geology, Eötvös Loránd University. The identification of probable organic matter was evaluated using a Zeiss microscope equipped with an Hg vapour lamp and filters for blue light excitation (450–490 nm) at the MTA-ELTE Geological Research Group. In this equipment the filter set is composed of a diachromatic beam splitter (510 nm) and a barrier filter (515 nm). Backscattered electron microscopy (SEM) was carried out on an Amray, 1830i instrument (Amray, Bedford, MA, US) equipped with INCA Energy-dispersive X-ray spectrometer (EDS) at the Department of Petrology, Eötvös Loránd University.

Stable isotope measurements were performed on micro-drilled powders of carbonate samples, at the Institute for Geological and Geochemical Research. The analyses were carried out using the

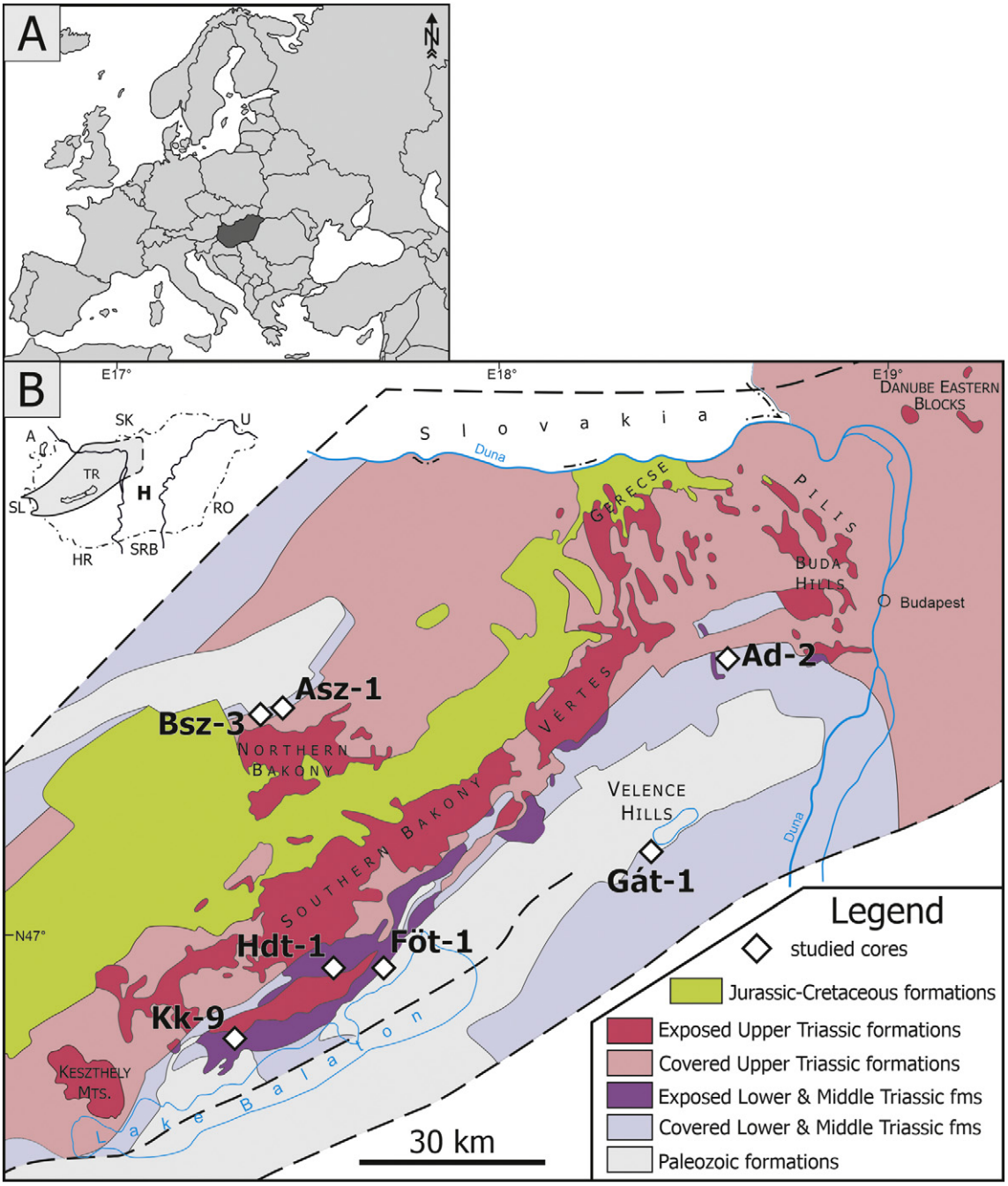

Fig. 1. Geological map of the investigated area. (a) Location of Hungary in Europe, (b) Position of the studied cores on the pre-Cenozoic geological map of the Transdanubian Range (Haas et al., 2004), the index figure indicates the position of the Transdanubian Range in Hungary (A: Austria, SK: Slovakia, U: Ukraine, RO: Romania, SRB: Serbia, HR: Croatia, SL: Slovenia. Wells: Asz-1: Alsószalmavár-1, Bsz-3: Bakonyszűcs-3, Kk-9: Köveskál-9, Hdt-1: Hidegkút-1, Föt-1: Felsőörs-1, Gát-1: Gárdony-1, Ad-2: Alcsútdoboz-2).

continuous flow technique (Spötl and Vennemann, 2003), using different reaction times for calcite and dolomite samples (Rosenbaum and Sheppard, 1986). $^{13}C/^{12}C$ and, $^{18}O/^{16}O$ ratios were determined in CO_2 gases liberated by phosphoric acid using a Finnigan delta plus XP mass spectrometer (Thermo Fisher Scientific, Bath, UK). Standardisation was conducted using laboratory calcite standards calibrated with the NBS 18, NBS 19 and LSVEC standards. During measurement of the dolomite samples a laboratory dolomite standard (DST) was used. All samples were measured at least in duplicate and the mean values are in the traditional δ notation in parts per thousand (‰) relative to Vienna Pee Dee Belemnite (VPDB). Reproducibility is better than ±0.1‰ for $\delta^{13}C$ and ±0.15‰ for $\delta^{18}O$. Part of the stable isotope data was published previously in Haas et al. (2017).

4. Results

The studied Lower Triassic successions comprise limestones, dolomites, sandstones and siltstones. Rock types containing siliciclastic and carbonate components (hybrid arenites or marls) are also common. The analysed sedimentary units contain calcite, dolomite, clay minerals and quartz in variable amounts. The main characteristics of the rocks are summarized in Table 1 on Haas et al. (1988); Broglio Loriga et al. (1990) and our own observations. The mineralogical composition of the investigated cores and their lithological classification are summarized in Fig. 3.

Based on microscopic investigations five lithotypes (LT) were differentiated: dolomite (LT1), sandy, silty and clayey dolomite and dolomarl

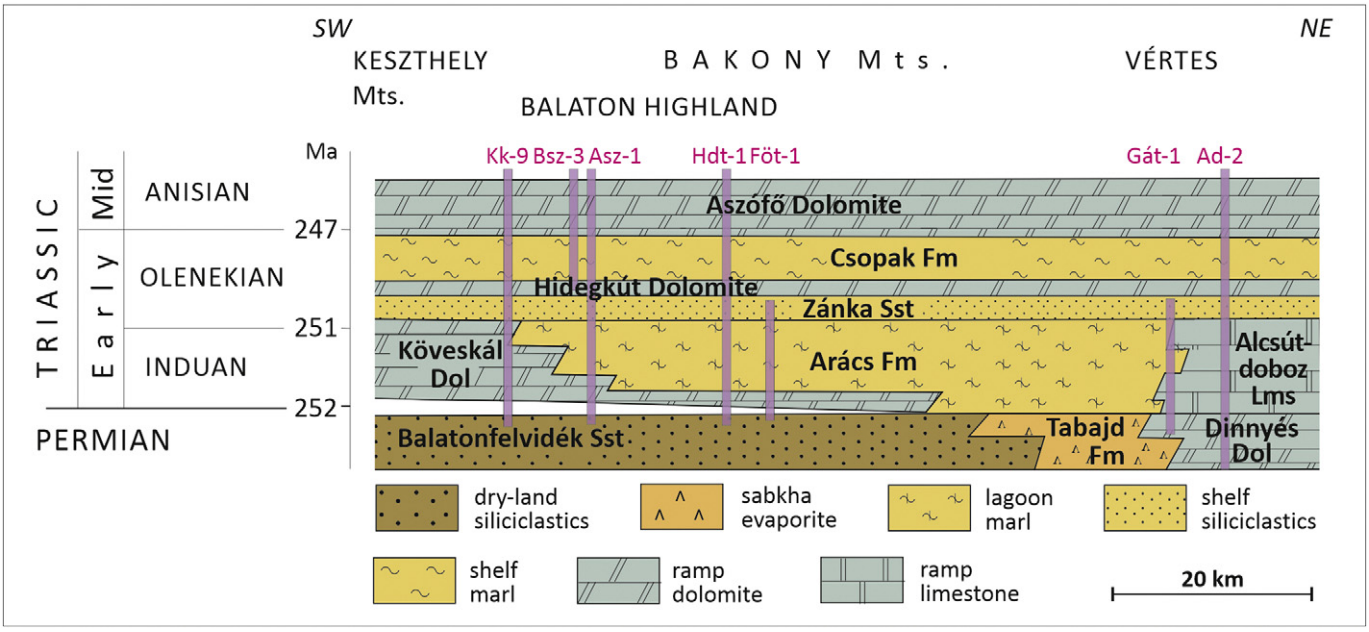

Fig. 2. Spatial relationships between the Upper Permian and Lower Triassic formations of the Transdanubian Range along a transect (Haas and Budai, 1999).

(LT2), dolomitic siltstone and sandstone (LT3), dolomitic limestone (LT4), and limestone (LT5). They appear in 0.5 to tens of meter thick intervals in the drill cores. These lithotypes are described in detail in the following sections. In the lithotype names sand, silt and clay refer to grain sizes.

4.1. Lithotypes

4.1.1. Lithotype, 1 (LT1): dolomite

In this lithotype two subtypes were differentiated based on the microtexture of the dolomites. They commonly appear together, usually interlayered with each other.

4.1.2. Lithotype, 1A (LT1A): fabric-destructive dolomite

LT1A has been identified in the Köveskál and Arács Formations (Table 1). Fabric-destructive dolomite containing less than 5% of siliciclastic components comprises this lithotype. The sedimentary fabric is completely obstructed due to replacement by planar-s and nonplanar-a dolomite (dol1) varying from 5 to 500 μm in size (Fig. 4a–d). Turquoise-stained, 10- to 200-μm-sized planar-s dolomite-ankerite crystals (dol2-ank) occur on dol1 as overgrowth cement adjacent to clay-rich zones (Fig. 4c). This ferroan dolomite-ankerite (dol2-ank) appears in an irregular vug-fracture system. Both dolomite types (replacive and overgrowth cement) show undulose extinction (Fig. 4b). Irregular-shaped, 50 to 500 μm-sized, vug pores, occur randomly (Fig. 4d) within these dolomites. This lithotype is, in some cases, associated with gypsum and subordinately with anhydrite in the wells from the northern part of the Transdanubian Range (Asz-1 and Bsz-3) (see below).

4.1.3. Lithotype, 1B (LT1B): fabric-retentive dolomite

LT1B, together with LT2 (see below) were described in the Köveskál Formation (wells Kk-9, Föt-1) (Table 1). Fabric-retentive dolomites containing less than 5% siliciclastic components comprise this lithotype. The replacive dolomite is characterized by very fine- to medium-crystalline, planar-s to nonplanar-a texture (dol1). The degree of fabric preservation varies. However, the original sedimentary fabric is typically recognizable (Fig. 5). Fragments of dolomitized echinoderms and syntaxial overgrowth cement are commonly observed (Fig. 5a,d). Shelter pores with coarse-crystalline replacive dolomite indicate the presence of mollusc shells (Fig. 5b). Ghosts of 300 to 500 μ-sized spheroidal particles suggest former ooid packstone/grainstone fabric (Fig. 5c). In some samples, either the outer rim of the dolomite crystal or the entire crystal is stained turquoise (dol2), indicating iron-content (Fig. 5d). Ankerite occurs as fracture- and vug pore-filling mineral (Fig. 5d). Dissolution seams or stylolites are common and marked by brownish goethitic material.

4.1.4. Lithotype, 2 (LT2): sandy, silty, clayey dolomite, and dolomarl

LT2 predominates in the Arács Formation, both in the Northern Bakony (well Asz-1) and Balaton Highland area (well Kk-9) (Table 1). Dolomitic rocks that contain 5 to 50% of siliciclastic components comprise this lithotype. The siliciclastic components are mainly quartz, quartzite, clay minerals, and mica. Either finely-crystalline, nonplanar-a, non-ferroan dolomite (dol1) or medium to coarse-crystalline, nonplanar-a, turquoise-stained, ferroan dolomite to ankerite (dol2-ank) appear between quartz, quartzite, and mica grains (Fig. 6a,b). In some cases, dol1 or dol2-ank poikilotopically encloses the quartz grains that are “floating” in the dolomite, which suggests an original matrix-supported fabric (Fig. 6b). Dol1 and dol2-ank are commonly brownish in plane-polarized light due to the large numbers of small (in size few μm) solid inclusions. Both exhibit undulose extinction (Fig. 6b) and no growth zonation were observed in cathodoluminoscope and scanning electron microscope. Rhombic dolomite cement crystals (dol3) filling/lining pores were also observed. Anhydrite (anh1) poikilotopically encloses dolomite (dol1, dol2-ank) crystals, and also fills the pore spaces that remained open after the precipitation of the dol3 crystals. Glauconite grains that are 10 to 100 μm-sized occur along pressure dissolution seams and stylolites (Fig. 6c), and are commonly associated with opaque minerals. In sandy dolomite, gypsum occurs as nodules enclosing nonplanar-a dolomite crystals and quartz grains. Curved flakes of mica are more abundant in certain beds. The mica is occasionally surrounded by hematite. This lithotype contains 1 to 10 mm-sized vug pores (Fig. 6d). The rocks commonly exhibit a laminated structure, although the laminae are often disturbed. Some laminae are rich in quartz grains, whereas others consist mostly of dolomite and mica. Low-amplitude stylolites cut across these rocks.

Table 1
Characteristics of the Lower Triassic formations of the Transdanubian Range. The information is compiled from Haas et al. (1988) and Broglio Loriga et al. (1990). The classification of the lithotypes is based on petrographic investigations of this study.

		Age	Rock types	Colour of the rocks	Sedimentological features	Fossils	Depositional environment	Clay minerals	Lower boundary	Upper boundary	Thickness	Lithotypes
Csopak Marl Formation		Olenekian	calcareous marl, marl, silty marl, siltstone	lower unit with grey marl, calcareous marl, middle unit with red, calcareous siltstone, upper unit with greenish grey silty marl and sandy marl	parallel stratification, uneven bedding planes, bioclastic limestone in lenses (eroded top), bioturbation (except the red intervals), coquinas (with pore-filling glauconite)	molluscs, microgastropods, foraminifers	open marine, low-energy environment with occasional storm events, quiet subtidal zone, below the fair-weather wave-base	illite group is predominant (in the middle, red unit chlorite is always associated)	continuous transition from the underlying Hidegkút Formation	overlain by Middle Triassic dolomite	50–250 m	1, 4, (2)
Hidegkút Formation	Hidegkút Dolomite Member	Olenekian	dolomite, evaporitic dolomite	grey	parallel bedding with planar bedding planes, oolites (occasionally with pore-filling glauconite)	rare (only microflora, that is similar to that of the underlying beds)	subtidal zone (restricted lagoon?)	-	sharp contact with the underlying Hidegkút Sandstone	continuous or well-defined boundary towards the overlying Csopak Formation	30–40 m	1, 2
	Zánka Sandstone Member	Early Olenekian	siltstone, sandstone	red, the pelite-rich bioturbated intervals are grey	parallel bedding with planar to ripple lamination, bioturbation (mostly horizontal burrows, occasionally U-shaped or vertical burrows)	sporomorphs foraminifers molluscs	subtidal zone of the inner-shelf, below the fair-weather wave-base	illite group is predominant	transition from the underlying Köveskál, Arács and Alcsútdoboz Formations (gradual change in the colour and carbonate content)	sharp contact towards the overlying Hidegkút Dolomite	40–50(–140) m	2, 3, (1)
Alcsútdoboz Limestone Formation		Induan	limestone, calcareous marl, silty marl with dolomite, dolomarl, dolomitic siltstone intercalations	grey	thin intercalations of (glauconitic) gastropode oolite, calcarenite and crinoidal or mollusc shell coquinas, laminated marls with loaded to slump horizons, micronodular limestones	sporomorphs calcareous algae foraminifers molluscs	inner shelf	illite group is predominant	continuous transition from the underlying Permian evaporites	sharp contact towards the overlying Hidegkút Formation	150–200 m	4, 5
Arács Marl Formation		Induan	limestone, calcareous marl, dolomite, sandy dolomite	grey, yellowish grey, red	microlamination, ripple marks, wavy bedding, gastropode oolite layers, bioturbation (vertical and U-shaped burrows)	sporomorphs foraminifers molluscs	intertidal zone and subtidal zone, below the fair-weather wave-base	kaolinite and illite in nearly equal amounts	erosional contact towards the underlying Permian sandstone or continuous development from the underlying Köveskál Formation	continuous transition towards the overlying Hidegkút Formation	80–120 m	1, 2, (3)
Köveskál Dolomite Formation		Induan	dolomite, dolomitic marl	grey with occasional red marl layers	parallel stratification, thin bedded or laminated, horizontal burrows (weak bioturbation), shrinkage cracks and evaporite nodules are typical in the north and west, (glauconitic) bioclastic grainstone lenses	sporomorphs foraminifers ostracods molluscs	low-energy inner shelf or lagoon, intertidal and subtidal zone	mainly kaolinite in the south, illite in the north	erosional contact towards the underlying Permian sandstone	overlain by the Lower Triassic Hidegkút Formation, the transition is continuous	80–120 m	1, 2, (3)

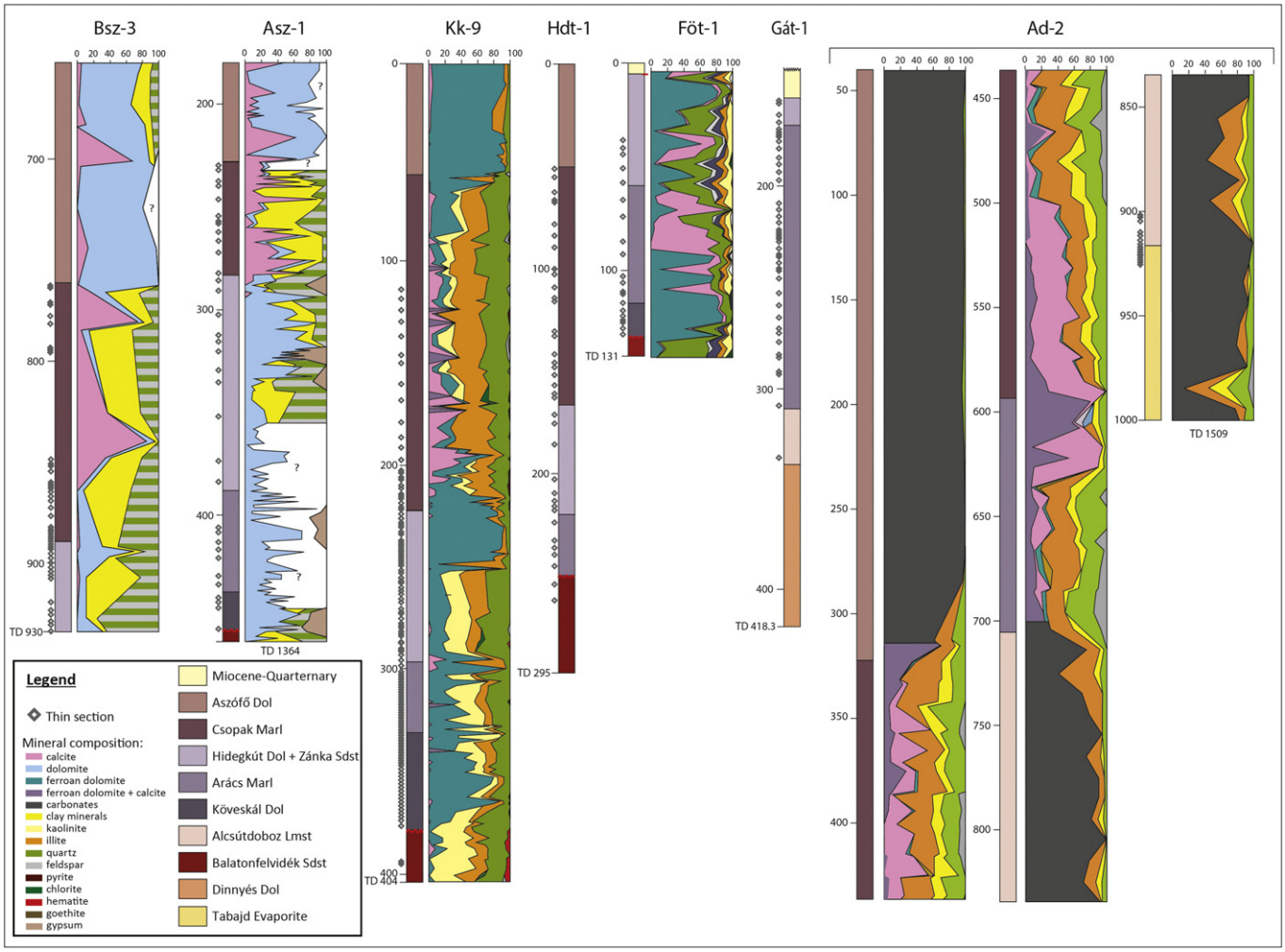

Fig. 3. Mineralogical composition and stratigraphic assignment of the investigated cores, redrawn from archive unpublished reports.

4.1.5. Lithotype 3 (LT3): dolomitic siltstone and sandstone

This lithotype typically occurs in the Olenekian rocks (Hidegkút Fm., wells Bsz-3 and Asz-1) (Table 1). Dolomitic siltstones and sandstones contain more than 50% of sand and silt-sized siliciclasts; which mostly corresponds to quartz, quartzite grains, and subordinate feldspar and mica. The quartz is present as angular to sub-rounded grains 10 to 100 μm (up to 900 μm) in diameter (Fig. 7). The grains show point contact or occasionally sutured grain contact. The larger grains are rounded and some of them are fractured (Fig. 7a), while the smaller grains have irregular boundaries and serrated contacts (Fig. 7b,c). The quartz grains show red to brownish luminescence (Fig. 7c). A few-μm-thick, non-luminescent overgrowth cement rim (qz1) can be observed on quartz grains. In some cases, both the grain and the overgrowth cement are cut across by quartz veins (qz2).

Replacive, nonplanar-a, non-luminescent, 100 to 500-μm-sized ferroan dolomite-ankerite crystals (dol2-ank) fill oversized pores between quartz grains that are not connected to each other in two dimensions (Fig. 7a–c). Planar-s ferroan dolomite-ankerite (dol2-ank) was also observed, growing into vugs with anhydrite filling the remaining space (Fig. 7a). Planar-s ferroan dolomite-ankerite (dol2-ank) is also present as a poikilotopic cement phase, enclosing quartz grains (Fig. 7b). These crystals are stained turquoise to blue and compositional zonation was revealed by energy-dispersive spectrometer of the electron microscope. Each zone contains different amounts of Ca, Mg, Fe, and Mn and, based on the composition, these zones can be classified as ferroan dolomite and ankerite (Fig. 7e,f, Electronic supplementary material). In some cases, the zone boundaries are irregular, and some zones appear patchy (Fig. 7f). Dol2-ank crystals are characterized by undulose extinction. The partly mottled, and partly zoned appearance of dol2-ank suggests that they are present both as replacive and as a cement phases.

Kaolinite occurs between the quartz grains, in amounts locally exceeding the amount of the carbonate constituents (Fig. 7d). Where clay minerals are present, the carbonates stain blue, indicating higher iron content than that of the purple-stained phases. Furthermore, sulphides (such as pyrite, chalcopyrite, galena and sulphosalts) are also associated with this lithotype. The siltstone and sandstone contain less than 5% mica. The mica flakes are occasionally surrounded by brownish to reddish iron-oxide rims and/or clay minerals (illite – Fig. 7f). Subordinately K-feldspar, zircon, apatite, and titanite were also observed. The rocks are rich in irregularly-shaped secondary pores (20 and 500 μm) that cut across through quartz, carbonate, and clay minerals.

The sandstones and siltstones (Zánka Member) of the Hidegkút Formation are commonly rich in clay minerals, ankerite, and ferroan calcite (Fig. 7e). The ankerite and ferroan calcite exhibit growth zoning and may occur among quartz grains, replacing bioclasts or in a few mm-sized fractures and vugs.

4.1.6. Lithotype 4 (LT4): dolomitic limestone

LT4 is present in all wells studied. The dolomitic grainstones are typical in the Arács and Hidegkút Formations. Dolomitic wackestones and packstones with minor siliciclast content occur in the Arács and Csopak Formations (Table 1). This lithotype includes wackestones, packstones and grainstones (Fig. 8a–c). The grainstones consist of

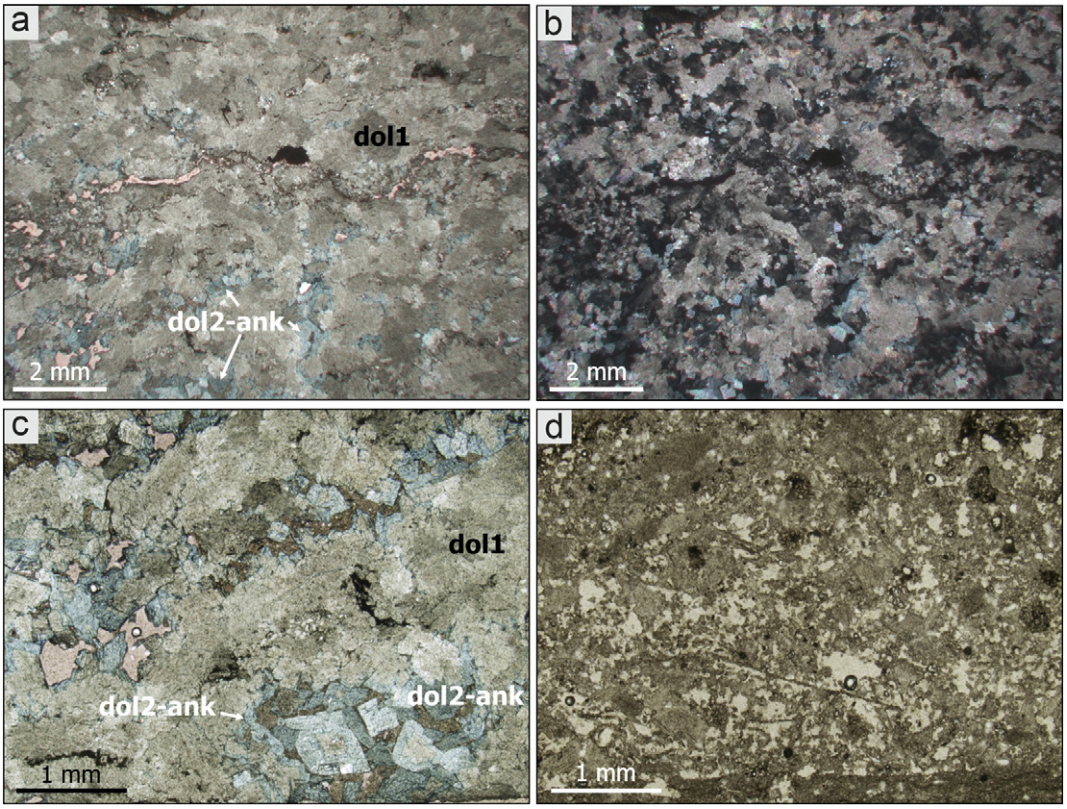

Fig. 4. Photomicrographs of fabric-destructive dolomites, LT1A. (a) Nonplanar-a, non-ferroan (dol1) to planar-s turquoise-stained ferroan, coarse-crystalline dolomite-ankerite (dol2-ank), well Föt-1 70.0 m, Arács Fm., stained thin section, plane-polarized light (PPL). (b) Same as "a" in cross-polarized light (XPL) showing the undulose extinction of the dolomite crystals. (c) Nonplanar-a, non-ferroan dolomite (dol1), and ferroan dolomite-ankerite overgrowth (dol2-ank), adjacent to brownish, clay-rich zones, well Föt-1 70.0 m, stained thin section, PPL. (d) Vug pores in dolomite (dol1), well Kk-9 356.2 m, PPL. (For interpretation of the references to colour in this figure legend, the reader is referred to the web version of this article.)

ooids and bioclasts (mostly gastropods), which are cemented by calcite and ferroan calcite (Fig. 8a–c). The bioclasts are commonly surrounded by a thin fibrous calcite rim, whereas the remaining pore-space is filled with drusy calcite and ferroan calcite (Fig. 8a,b). The bioclasts are partly replaced by 30 to 400 μm-sized, planar-e to nonplanar-a ferroan dolomite to ankerite crystals (dol2-ank) that often show undulose extinction (Fig. 8a–d). Clay minerals were found in the dolomitized domains. Staining colour of the dolomite-ankerite phases is more bluish where clay minerals are present. Black organic matter, together with fine pyrite crystals, occur along growth zones of dol2-ank crystals and filling the intercrystalline pore space between dissolved dol2 crystals (Fig. 8d). Locally, the planar-e dol2-ank crystals have a dark brownish outer rim, composed of goethite. Calcitic zones and patches occur in dol2-ank crystals (Fig. 8e). Anhedral quartz crystals, 10 to 20 μm in size, are relatively abundant in this lithotype and occur within bioclasts and between the grains (Fig. 8b). In some samples, quartz fills secondary pores (Fig. 8f). Anhedral quartz and dolomite occur along stylolites, as well, and are cut-across by ferroan calcite veins (Fig. 8c).

4.1.7. Lithotype 5 (LT5): limestone

This lithotype occurs in the Alcsútdoboz and Arács Formations, mainly in the north-eastern part of the Transdanubian Range (wells Ad-2, Gát-1) (Table 1). This lithotype encompasses nodular mudstone, bioclastic wackestone and grainstone. (Fig. 9a–d). In the grainstones spheroidal grains, peloids, and bioclasts (calcareous algae, foraminifers, molluscs, ostracodes, brachiopods, and echinoderm fragments) occur. Some bioclasts and other grains are surrounded by a micritic envelope (Fig. 9a,c,d). The remaining pore spaces between the grains are filled with drusy non-ferroan and ferroan calcite (Fig. 9b–d). The spheroidal grains are composed of 30 to 400 μm-sized calcite or ferroan calcite crystals that exhibit growth zonation, undulose extinction and subordinately curved crystal planes (Fig. 9c,d). In some cases, the concentric structure of the ooids has been preserved and only the central part of the grains is replaced by coarse-crystalline calcite (Fig. 9b). Stylolites, marked by anhedral quartz and brown dissolution residue, are common.

4.2. Sulphate and sulphide minerals in the Lower Triassic rocks

Gypsum and anhydrite commonly occur in LT1A, LT2 and LT3, in the Northern Bakony.

Gypsum occurs in six forms:

- Poikilotopic gypsum crystals (gp1) that form patches in LT2 and LT3 (Fig. 10a);
- Fibrous gypsum crystals (gp2) that fill fractures and anastomosing vugs in LT1A and LT2 (Fig. 10b), and have irregular boundaries towards both the quartz and the dolomite;
- Equant gypsum crystals (gp3) that fill the pore space among bioclasts (Fig. 10c);
- Nodular gypsum (gp4), occasionally enclosing 5 to 200 μm-sized anhydrite crystals in LT2 and LT3 (Fig. 10d);
- Nodules, composed of ca. 100-μm-sized gypsum crystals (gp5) that have serrated, irregular boundary (Fig. 10e). These types of nodules often contain 50 to, 200 μm-sized irregularly-shaped dolomite inclusions and are typical in LT2 and LT3;
- Coarse-crystalline, anhedral gypsum (gp6) observed as pore-fill phase in fabric-retentive dolomites (LT1B), and also present as a fracture-fill post-dating coarse-crystalline dolomite (Fig. 10f).

Anhydrite is common in the dolomitic sandstones of the Zánka Sandstone Member (LT1, LT2, and LT3). It fills anastomosing vugs and poikilotopically encloses dolomite crystals (Fig. 11a–d). Pore-filling

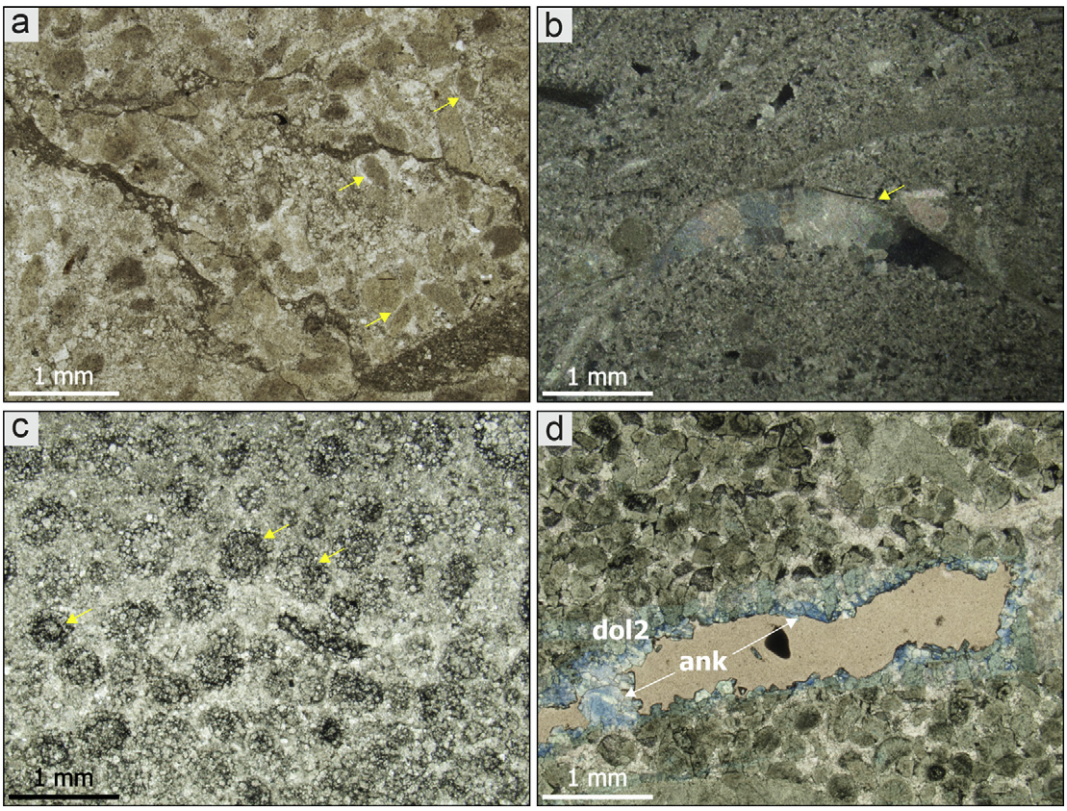

Fig. 5. Photomicrographs of fabric-retentive dolomites, LT1B. (a) Fine- to medium crystalline, planar-s dolomite with bioclastic packstone fabric. Note the syntaxial overgrowth cement on the echinoderm fragments (yellow arrows). Well Asz-1, 245.0 m, Csopak Fm., PPL. (b) Fine- to coarse-crystalline, planar-s dolomite with bioclastic wackestone fabric. Coarse-crystalline replacive dolomite in a shelter pore under the mollusc shell (indicated by yellow arrow) exhibits undulose extinction. Well Asz-1, 263.7 m, Csopak Fm., cross-polarized light (XPL). (c) Coarse crystalline, planar-s dolomite with ooid packstone/grainstone fabric suggested by ghosts of sand-sized, micritized particles (indicated by yellow arrows). Well Föt-1, 130.5 m, Köveskál Fm., plane-polarized light (PPL). (d) Dolomitized bioclastic grainstone with fragments of echinoderms. Blue-stained ankerite (ank) lines the vug pore. Well Föt-1 42.3 m, Hidegkút Dolomite, stained thin section, PPL. (For interpretation of the references to colour in this figure legend, the reader is referred to the web version of this article.)

anhydrite surrounds and thus, post-dates euhedral dolomite crystals (Fig. 11b), and is intergrown with poicilotopic gypsum (gp1) (Fig. 11c, d).

Barite fills secondary pores and hairline fractures in LT1A and LT2 (Fig. 12a–c). Lath-shaped barite crystals (Fig. 12a) occur in 1 mm-sized patches within dolomites. These patches are rich in disseminated, and a few μm-sized pyrite. The lath-shaped barite crystals typically enclose 10 to 100 μm-sized, planar-e to planar-s ferroan dolomite-ankerite crystals (Fig. 12b). Where ankeritic rims of dol2 crystals occur, these rims are corroded towards the barite (Fig. 12b). In some cases, the barite encloses kaolinite (Fig. 12c) and is also associated with sulphosalts in vugs (Fig. 12d).

Two types of pyrite were found in the studied Lower Triassic rocks. Anhedral pyrite crystals, up to 100-μm in size, occur along the boundary between organic-matter-rich and poor horizons and in micropores of echinoderm fragments (Fig. 13a,b,c). In the micropores of the echinoderm fragments pyrite postdates dol3. Pyrite also appears as 1 to 2 mm-sized scattered euhedral crystals. Elongated, 30 to 80-μm-sized dolomite inclusions occur along zones within the pyrite crystals (Fig. 13d).

Sulphosalts were found in, irregularly-shaped pores of up to 100-μm size in LT1A and LT2 (Fig. 12d). The main elements determined by EDS in the sulphosalts are Cu, Sb, Zn, As, and Hg. Anhedral galena and chalcopyrite, up to 30-μm-sized occur as irregularly-shaped inclusions in the sulphosalts.

4.3. Stable isotope geochemistry

The stable oxygen and carbon isotope pattern of the Lower Triassic rocks are characterized by rather negative $\delta^{18}O$ and both negative and positive $\delta^{13}C$ values (Fig. 14, Electronic supplementary material). The $\delta^{18}O$ values of dol1 are from −9.3 to −5.8‰, whereas the $\delta^{13}C$ values range from −1.9 to +2.5‰. Dol2 is characterized by a wider range of isotope values ($\delta^{13}O = -10.7$ to −4.2‰ and $\delta^{18}C = -4.8$ to +4.7‰). It was not possible to sample dol3 selectively. The limestone samples (LT5) are composed of calcite and ferroan calcite and show a relatively narrow isotope range ($\delta^{18}O = -10.5$ to −7.7‰ and $\delta^{13}C = +0.1$ to +2.0‰). The ferroan calcite, present in the dolomitic limestones samples (LT4) fall within the range of dol2 values ($\delta^{18}O = -7.6$ to −6.7‰ and $\delta^{13}C = -2.9$ to +1.7‰). Only one ferroan calcite vein was possible to sample, and that data point shows the most negative $\delta^{18}O$ values (−15.2‰), and a $\delta^{13}C$ value of +0.5‰.

5. Discussion

5.1. Paragenetic sequence

A paragenetic sequence of the diagenetic minerals is given in Fig. 15 and is based on cross-cutting relationships. Most of the detected mineral phases could be related to the different dolomite types and therefore their relative sequence can be determined, but none of the lithotypes contains all the diagenetic events. Diagenetic event and the resulting mineral phases are related to the lithotypes in Fig. 15. Further local differences in the sequence are described below.

Three types of dolomites were differentiated in the investigated rock types: (i) replacive non-ferroan dolomite (dol1), (ii) replacive ferroan dolomite-ankerite (dol2-ank), and (iii) ferroan dolomite-ankerite cement (dol3). Dol1 is only present in LT1 and LT2, where dol2 and then dol3 phases postdate it (cf., Fig. 4a,c). Dolomitization in LT1 and LT2 appears to be the first detectable diagenetic process. In LT3, a quartz

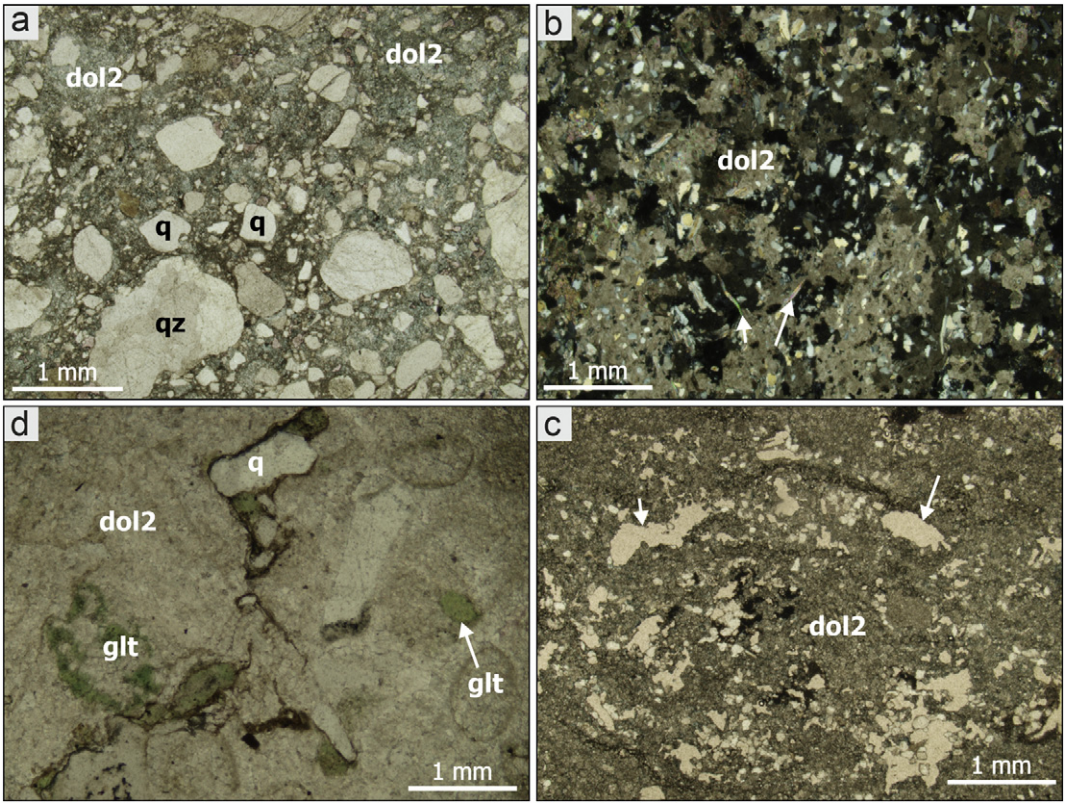

Fig. 6. Photomicrographs of sandy and silty dolomites, LT2. (a) Turquoise-stained, ferroan dolomite-ankerite (dol2-ank) in-between quartz (q) and quartzite (qz) grains. Brownish areas are rich in clay minerals. Well Asz-1 374–375 m, Zánka Sandstone, stained thin section, plane-polarized light (PPL). (b) Quartz, quartzite grains and mica flakes (white arrows) enclosed by poikilotopic nonplanar-a dolomite (dol2), well Kk-9 373.9 m, Köveskál Fm., XPL. (c) Glauconite (glt) in the vicinity of stylolites marked by brown Fe-oxide in nonplanar-a dolomite (dol2), Well Asz-1, 448 m, Arács Fm., PPL. (d) Vug pores in nonplanar-a finely-crystalline dolomite (dol2), well Kk-9 333.5 m, Arács Fm., PPL. (For interpretation of the references to colour in this figure legend, the reader is referred to the web version of this article.)

overgrowth cement (qz1) was observed on the quartz grains (Fig. 7d), furthermore both the grains and the cement are cut by fractures filled with quartz cement (qz2). The poikilotopic dolomite (dol2-ank) encloses these quartz components (Fig. 7c).

The samples from the northern part of the Transdanubian Range (Asz-1 and Bsz-3) contain both gypsum and anhydrite. The dolomite (LT1) is cross-cut by fractures with coarse dolomite cement (Fig. 10f). The remaining pore space in these fractures is filled with gypsum (Fig. 10f), whereas vug pores are filled with anhydrite (Fig. 11b) that is partially replaced by gypsum (Fig. 11d). Ferroan calcite replaces dolomite in the dolomitic limestone (LT4) (Fig. 8e), furthermore ferroan calcite veins cut across these samples, as the last diagenetic phase (Fig. 8c). The sulphate minerals and the ferroan calcite were not found together in the same sample; hence their relative age remains an open question. No sulphides were found in the presence of gypsum and anhydrite.

In the samples from the southern part of the Transdanubian Range, vugs in the dolomite (LT1) are filled with authigenic kaolinite that is enclosed by barite (Fig. 12c). The barite seems to be coeval with sulphosalts that contain galena, chalcopyrite, and pyrite inclusions (Fig. 12d). Illitization of the mica flakes is very common in LT2 and LT3 (Fig. 7f). Enrichment of less-soluble minerals, and dolomite crystals were locally found along stylolites (Fig. 8c).

Dolomitic limestones (LT4) are the most common lithotype in the samples taken from the basal part of the Triassic succession (Alcsútdoboz Fm.) in the NE part of the Transdanubian Range. Micritic envelope surrounds the original, aragonitic grains (bioclasts and ooids) (Figs. 8a, 9a,c,d). Coarse subhedral ferroan dolomite and ankerite crystals partly replace the calcite in the bioclasts and ooids and they locally contain black organic matter along growth zones (Fig. 8b,d). Later coarse crystalline ferroan calcite replaced the dolomite (Fig. 8e), in some cases leading to complete calcitization (LT5, Fig. 9c). Nonplanar-a replacive dolomite is also present along stylolites. Ferroan calcite also appears as a fracture fill both pre- and post-dating the stylolitization.

Point and sutured grain contacts in the sandstones (LT3), indicate that cementation by dol3 is post compactional (Fig. 7a–c).

5.2. Timing and mechanism of dolomitization

The petrographic features and isotope data suggest polygenetic dolomitization of the studied Lower Triassic rocks (Fig. 16). Bioclasts and ooids found in the fabric-retentive dolomite (LT1B) point to a shallow marine limestone precursor. Furthermore, the occurrence of gypsum and anhydrite in the Lower Triassic beds indicates arid conditions during deposition. Dolomitizing large masses of limestone during shallow burial is most effective via reflux processes, during which Ca^{2+} is removed from the seawater through precipitation of sulphates, therefore Mg^{2+}/Ca^{2+} in porewater increases (Tucker and Wright, 1990). Accordingly, dolomitization via reflux circulation of sea-water-derived high-density fluids in near-surface burial setting is supposed (Saller and Henderson, 1998; Machel, 2004; Johnes and Xiao, 2005; Al-Helal et al., 2012; Morad et al., 2012) (Fig. 16b). The observed replacive non-ferroan, nonplanar-a dolomite (dol1) likely belongs to this stage (Fig. 16d) as it is pervasively present and is accompanied by sulphate minerals. Relating genesis of dol1 to reflux processes corroborates with the Early Triassic aragonite sea (Gabellone and Whitaker, 2016), even though the $\delta^{18}O$ and $\delta^{13}C$ values of dol1 do not fall into the range expected for Triassic reflux dolomites (for Triassic marine calcite see Veizer et al., 1999; Korte et al., 2005).

In the case of LT1A, the dolomitization obscured the original limestone fabric. However, as this lithotype (LT1A) is interlayered with the fabric-retentive dolomite (LT1B), a shallow marine depositional

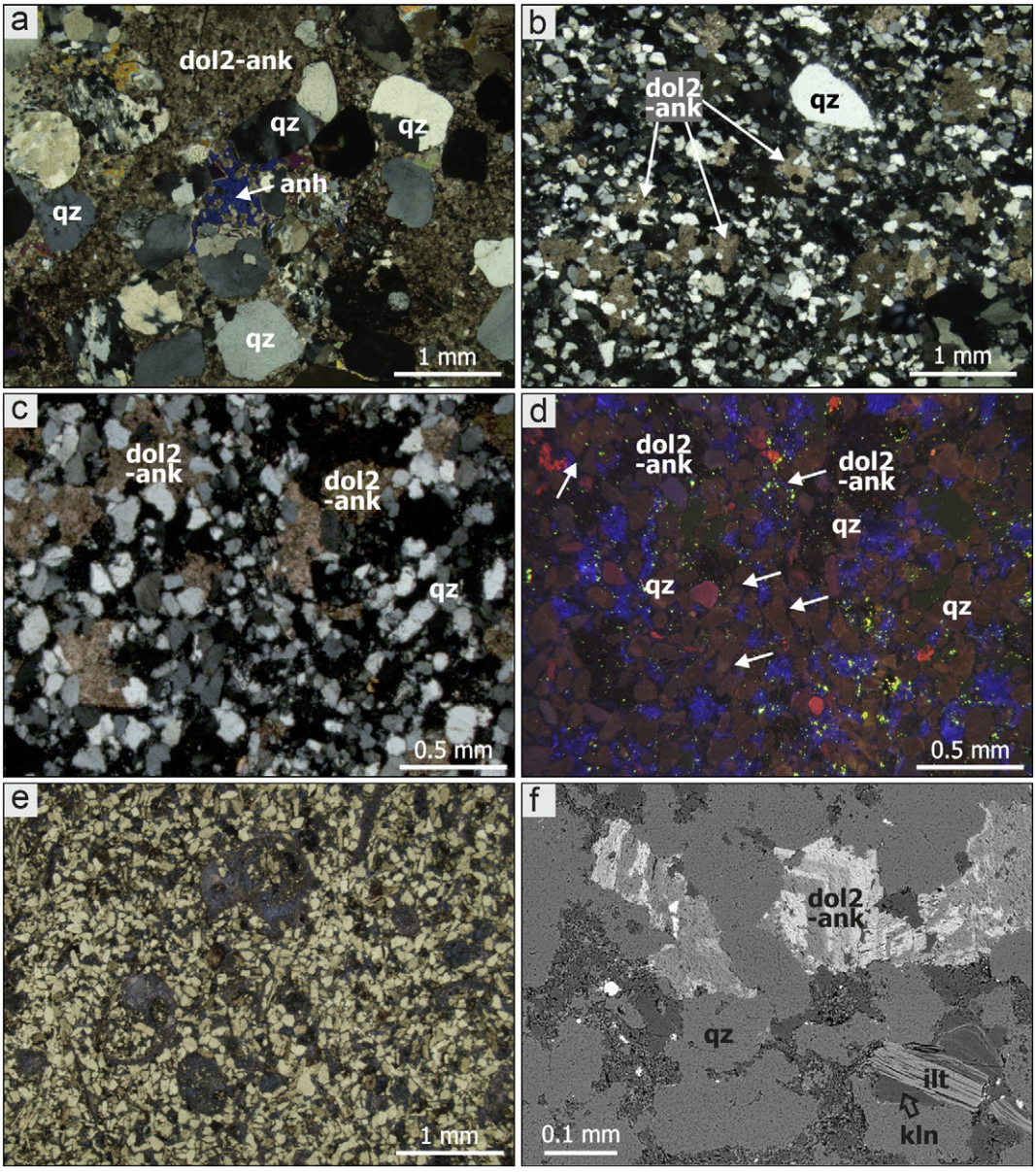

Fig. 7. Photomicrographs and BSE image of dolomitic siltstones and sandstones, LT3. (a) Anhydrite (anh), ferroan dolomite-ankerite (dol2-ank) between quartz and quartzite grains (qz), well Bsz-3 887.5 m, Hidegkút Fm., cross-polarized light (XPL). (b) Ferroan dolomite-ankerite (dol2-ank) poikilotopically enclosing quartz grains, well Kk-9 377.7 m, Köveskál Fm., XPL. (c) Ferroan dolomite-ankerite (dol2-ank) between quartz (qz) grains, well Kk-9, 377.7, Köveskál Fm., XPL. (d) CL image of c. Note the non-luminescent ferroan dolomite-ankerite (dol2-ank), the red-brown quartz grains (qz) with non-luminescent overgrowth (qz1, white arrows) and the blue luminescent kaolinite (e) Ferroan calcite (purple-blue) between angular quartz grains and mica flakes. The ferroan-calcite partly replaces bioclasts. Well Gát-1, 170.7 m, Arács Fm., stained thin section, plane-polarized light (PPL). (f) Backscattered-electron image showing zoned and mottled ferroan dolomite-ankerite (dol2-ank) in a silty sandstone. Kaolinite (kln) and illite (ilt) are also present between the quartz grains, well Kk-9 377.7 m, Köveskál Fm. (For interpretation of the references to colour in this figure legend, the reader is referred to the web version of this article.)

environment can be assumed for this, as well. The striking difference in the dolomite fabric (i.e., fabric-retentive vs fabric-destructive intervals) may reflect differences in the original depositional texture, i.e., higher porosity and permeability, the presence of fewer nucleation sites, etc. This can probably be attributed to the different parasequences, as highstand systems tract (HST) grainstones and packstones, testifying for sea-level highstands, are more excessively dolomitized compared to finer-grained transgressive systems tract (TST) limestones (cf., Morad et al., 2012).

As LT1 and LT2 are present spatially close to each other (in the Köveskál and Arács Fms.), the precursor phase of dol1 in LT2 was likely also deposited in shallow water, together with the siliciclastic grains. This is supported by the presence of gypsum. No remnants of precursor micrite or bioclasts were observed in the replacive dolomite, which suggests that either the replacive phase was completely fabric-destructive or both micrite and bioclasts were composed of aragonite, dissolved before dolomitization and reprecipitated as an early cement in the form of microcrystalline calcite, and these phases were subsequently replaced by dol1 (cf., Morad and De Ros, 1994). The early dissolution of bioclasts is supported by LT4 and 5 where the micritic envelope is preserving the shape of the dissolved grain formed soon after deposition (e.g., Tucker and Wright, 1990) and then drusy calcite filled the molds (Fig. 16d). This first replacive dolomite phase (dol1) is non-ferroan, suggesting a shallow burial setting where Fe^{2+} was not available to be incorporated in the calcite.

5.3. Burial dolomitization

Dol2 and dol3, found in LT2, LT3, and LT4, are closely associated with the barite and sulphide diagenetic phases, and indicate a subsequent

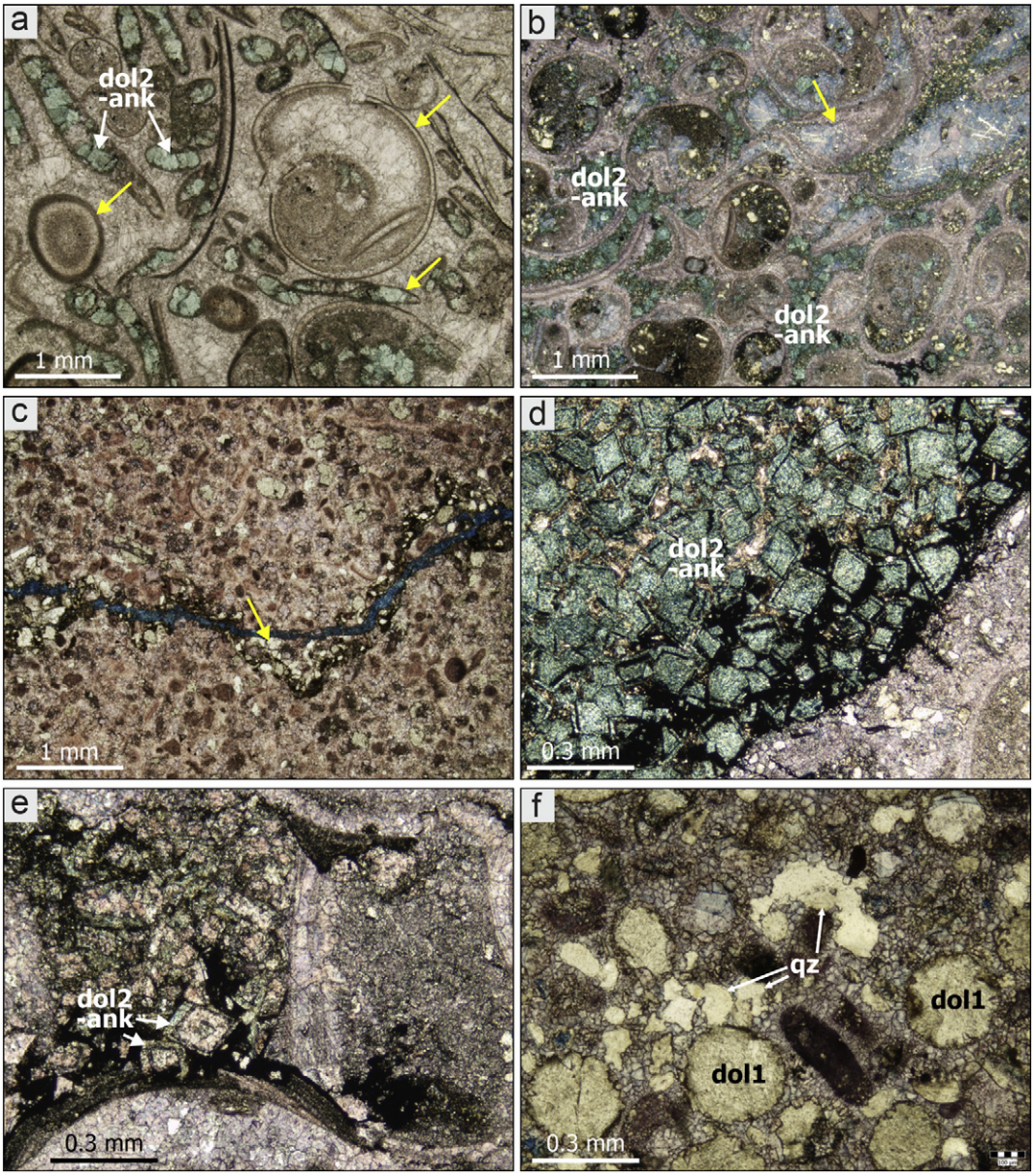

Fig. 8. Photomicrographs of dolomitic limestones, LT4. (a) Bioclastic grainstone. Micritic envelopes mark the outlines of the gastropods, which are filled with calcite and nonplanar-a turquoise-stained dolomite-ankerite (dol2-ank), well Gát-1, 277.6 m, Arács Fm., stained thin section, plane-polarized light (PPL). (b) Bioclastic grainstone. Planar-s, turquoise-stained dolomite-ankerite (dol2-ank) appears both in and among gastropods, locally accompanied by quartz and clay minerals. Quartz crystals are also present in the micrite within some bioclasts. Circumgranular bladed calcite cement surrounds the bioclasts. Vug pores are filled with purple-stained ferroan calcite exhibiting growth zonation (yellow arrow), well Gát-1, 167.6 m, Hidegkút Dolomite, stained thin section, PPL. (c) Quartz grains (yellow arrows) accumulated along a stylolite in a dolomitic limestone. The stylolite is cut across by a blue-stained ferroan calcite vein, well Ad-2 920.2 m, Alcsútdoboz Fm., stained thin section, PPL. (d) Black organic matter along the growth zones of planar-e to planar-s ferroan dolomite-ankerite (dol2-ank) crystals and between them, well Gát-1, 188.5 m stained thin section, PPL. (e) Partially calcitized (white arrows) planar-e, turquoise-stained dolomite-ankerite crystals (dol2-ank). Well Gát-1, 161.9, Hidegkút Dolomite, stained thin section, PPL. (f) Ferroan calcite among dolomitized ooids (dol1), secondary pores are filled with authigenic quartz (qz1). Well Ad-2, 917.4 m, Alcsútdoboz Fm., stained thin section, PPL. (For interpretation of the references to colour in this figure legend, the reader is referred to the web version of this article.)

event in the diagenetic history of the Lower Triassic rocks (Fig. 16c,d). The nonplanar-a crystals, the undulose extinction, the elevated iron and manganese-content, and low $\delta^{18}O$-values of dol2 and dol3, found in various lithotypes, suggest that they represent a relatively late replacive and cement phase, formed at elevated temperature and reducing conditions. Iron-rich carbonate cements are common in a number of argillaceous carbonates and carbonate-mudstone successions (McHargue and Price, 1982; Pye, 1985; Taylor and Sibley, 1986; Gregg, 1988). Since ferrous iron is not available in sufficient amount (0.02 ppm Fe) neither in the Mesozoic seawater, nor in the pore water during early diagenesis of the deposits, as long as organic matter is present (Richter and Fuchtbauer, 1978), another source should be taken into consideration. Where clay-rich strata are present interbedded with carbonate-rich strata, clay-derived Mg^{2+} is released via conversion of smectite to illite (Hower et al., 1976) or the dissolution of chlorite may contribute to the dolomitization. Therefore, iron and manganese may have been derived from clay minerals (Carrol, 1958; Oldershaw and Scoffin, 1967; McHargue and Price, 1982) or from other silicates, preserved in large amounts in LT2, and LT3. Smectite-illite transformation at around 125 °C can produce Ca^{2+}, Mg^{2+}, Fe^{2+} and water – all necessary for ferroan calcite, dolomite and ankerite formation (e.g., Boles and Franks, 1979; Hendry et al., 2000; Milliken, 2003; Meunier, 2005; Khalifa et al., 2018). The very variable Fe-, Mg-, and Mn-content of the carbonate phases (See electronic supplementary material and Fig. 7f)

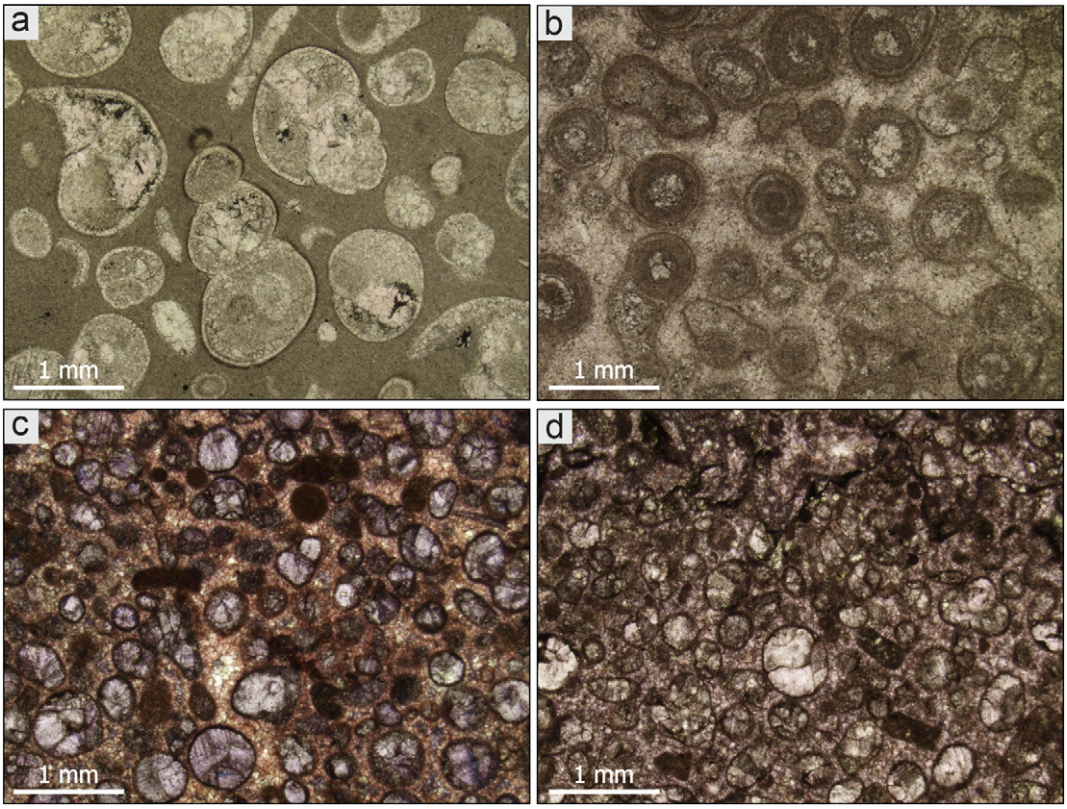

Fig. 9. Photomicrographs of limestones, LT5. (a) Bioclastic wackestone with gastropod shells filled with microspar and neospar/cement, some coated by micrite envelopes. Well Gát-1, 295.1 m, Arács Fm., stained thin section, plane-polarized light (PPL). (b) Ooidal grainstone, well Gát-1 336.4 m, Alcsútdoboz Fm., stained thin section, PPL. (c) Grainstone. Coarse-crystalline, anhedral, purple-stained, ferroan calcite occur in spheroidal grains that have micritic outline. The space between the grains is filled with non-ferroan calcite. Well Gárdony-1, 304.84 m, Arács Fm., stained thin section, PPL. (d) Grainstone. Coarse-crystalline, anhedral non-ferroan calcite occurs in spheroidal grains that have micritic outline. Non-ferroan calcite fills the space between the grains. Well Gát-1, 305.7 m, Arács Fm. stained thin section, PPL. (For interpretation of the references to colour in this figure legend, the reader is referred to the web version of this article.)

can be explained by the different amount and type of clay mineral cation sources. The highest iron content in the carbonate phases observed in the clay-rich Hidegkút and the Csopak Marl Formations, supports this hypothesis. Clay minerals can also adsorb hydrated iron- and manganese-oxides, which release metals under reducing conditions. Since phyllosilicates (mica and glauconite) are very common in the LT2 and LT3 lithotypes (Figs. 6b,d, 7f), they are the most plausible source for iron and manganese. Alternatively, these elements may have been derived from the iron oxides of the underlying Permian red sandstone. Reducing and alkaline pore water, rich in carbonate and poor in sulphate is needed for this process (Imam and Shaw, 1985).

The various dolomite types do not show separate clusters on the stable isotope cross plot and mostly fall outside the Early Triassic marine range (Fig. 14). The relatively uniform isotope data suggests either imperfect separation of dol1 from the other dolomite phases, or the signal of overprinting younger dolomite phases (dol2 and 3). Due to different oxygen isotopic fractionations during precipitation of calcite and dolomite (Fritz and Smith, 1970; Sheppard and Schwarcz, 1970; Land, 1980) the dolomite should be enriched in ^{18}O relative to calcite by approximately 2‰ to 4‰, meaning that the assumed marine dolomite fields were shifted to higher $\delta^{18}O$ values compared to the marine calcite fields (Fig. 14) Since the majority of the data fall out of this assumed marine dolomite range (Fig. 14), a different dolomitizing fluid is proposed. This interpretation is supported by low $\delta^{18}O$ values of all dolomite types that may have been caused by temperature dependent fractionation of oxygen isotopes between the cement phase and the fluid resulting from elevated temperature during burial diagenesis (cf., Anderson and Arthur, 1983; Moore, 1997). Or, alternatively by contribution of fluids from clay mineral dewatering (Coplen and Hanshaw, 1973) during diagenesis. Organic derived CO_2 in pore-water could result in low $\delta^{13}C$ values of the precipitating carbonate, as LT2 is quite rich in organic matter (cf., Irwin et al., 1977; Machel et al., 1995; Moore, 1997).

The ferroan dolomite and ankerite replacive and cement phases (dol2–3 and ank) indicate that early dolomitization (represented by dol1) was followed by a second dolomitization event. Elsewhere, recrystallization of dolomite into ferroan-dolomite or replacement by ankerite was reported previously (Schmid, 2004). This process has been also pointed out by geochemical modelling (Blomme et al., 2015). Such processes might have been responsible for the formation of ferroan dolomite and ankerite in the studied Lower Triassic succession. Furthermore, iron-rich dolomite commonly forms during mesodiagenesis (Boles, 1977; Pye and Krinsley, 1986; Sullivan et al., 1990; Souza et al., 1995; Anjos et al., 2000; Hendry et al., 2000; Elias et al., 2007). Ankerite has been often reported forming in association with thermal decarboxylation of organic matter and clay mineral transformations (Kantorowicz, 1985; Macaulay et al., 1993; Hendry et al., 2000). Thermal degradation of organic matter could provide CO_2 for carbonate cementation (Smith and Ehrenberg, 1989). Although shallow diagenetic ankerite (formed in mudrocks) has been also reported (Irwin et al., 1977), its intermediate to deep burial origin (related to the oil window) is more common. Dol3 in LT3 postdates both quartz overgrowth cement (qz1) and quartz-filled fractures (qz2), crosscutting both the grains and the overgrowth (Fig. 16d). This indicates that the physical compaction should have started prior to precipitation of qz2. The sutured grain contacts between quartz grains suggest internal Si source for qz1 and qz2 cement phases. However, silica produced by smectite-illite transformation reaction has been also available for the quartz overgrowth (Boles and Franks, 1979). Based on the above

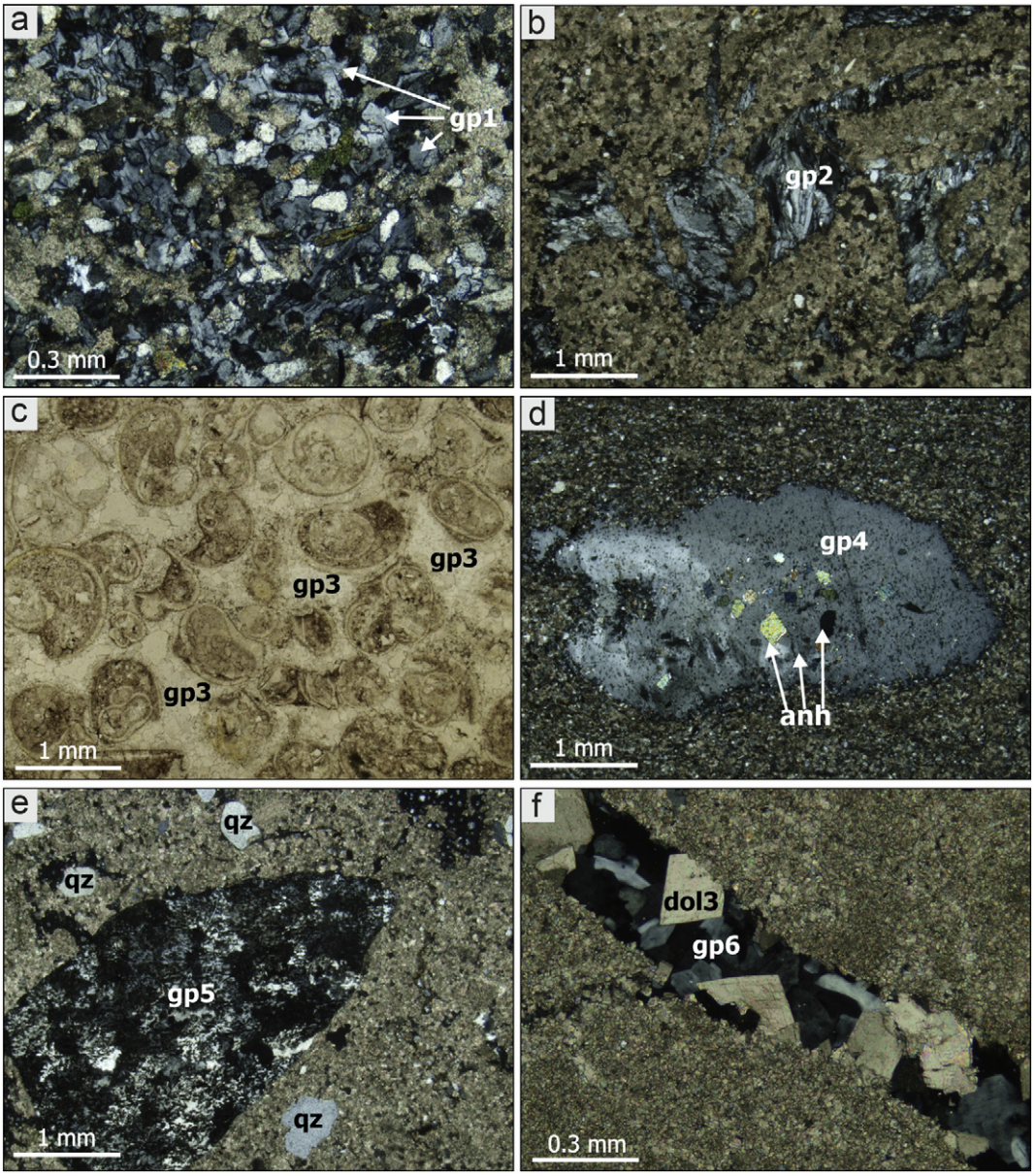

Fig. 10. Photomicrographs of the different types of gypsum. (a) Gypsum (gp1) in silty carbonate, poikilotopically hosting dolomite crystals, quartz and glauconite grains, LT2, well Asz-1, 425.5 m, Arács Fm., cross-polarized light. (b) Fibrous gypsum (gp2) filling vugs in fabric-destructive dolomite, LT1A, well Asz-1, 407.6 m, Arács Fm., cross-polarized light (XPL). (c) Bioclastic carbonate with gypsum (gp3) as the last pore-filling phase, LT1B, well Kk-9, 295.8 m, Zánka Sandstone, plane-polarized light (PPL). (d) Gypsum nodule (gp4) in silty dolomite, hosting remnants of anhydrite crystals, LT2, well Asz-1, 437.4 m, Arács Fm., XPL. (e) Gypsum nodule (gp5) in sandy and silty dolomite, LT2. Note the irregular boundaries between the gypsum crystals within the nodule, well Asz-1, 448.0 m, Arács Fm., XPL. (f) Fracture in fabric-destructive dolomite, filled with coarse-crystalline, subhedral dolomite (dol3) and gypsum (gp6), LT1A, well Hdt-1, 190.0 m, Hidegkút Dolomite, XPL.

considerations this stage of dolomitization postdates shallow burial stage. Quartz overgrowth commonly requires temperature higher than 60 °C (McBride, 1989). As dol3 is later than qz1 and qz2, all the above considerations suggest that the sandstones were dolomitized during medium to deep burial. The presence of dol2-ank and dol3 phases in all the lithotypes except the limestone (LT5) implies that they were a result of a larger scale, regional, fluid migration event.

5.4. Barite-sulphide mineralization

Co-occurrence of barite and sulphosalts constrains a discrete mineralization event postdating dol2 and dol3 (Figs. 12b, 16d). This event is restricted to the Lower Triassic formations. Traces of barite, galena and chalcopyrite, however, were also reported from the underlying Permian red sandstone (Majoros, 1998). Potential Fe sources for pyrite and sulphosalts can be the Fe-bearing clay minerals (such as biotite, glauconite, smectite, chlorite). The postdating relationship of sulphides to the ferrous carbonates suggests that by the time of barite and sulphosalt precipitation, Ca and Mg was not available anymore, as they were incorporated into the carbonate phases.

Sulphur could have been sourced from evaporites, present in the studied formations. Anhydrite and gypsum occur in the Lower Triassic beds, but mostly in the northwest part of the investigated area (Northern Bakony –, Szigliget-1 borehole – Budai et al., 1999), whereas the mineralization was mainly observed in the Balaton Highland region. This areal distribution pattern suggests the replacement of gypsum by barite and sulphide minerals, or at least local source of sulfur, in the latter region.

Barite originates from the mixing of reducing, barium-rich fluids with sulphate-rich fluids (Canet et al., 2013). Since barite and

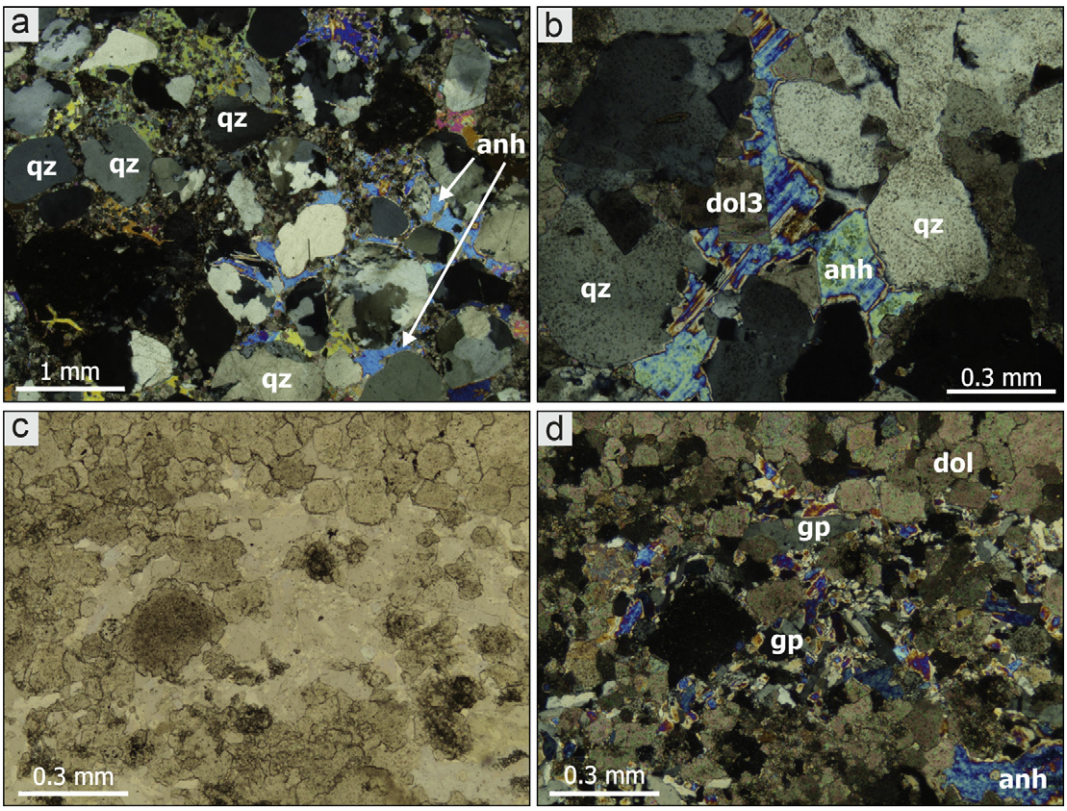

Fig. 11. Photomicrographs of anhydrites. (a) Poikilotopic anhydrite (anh) in sandstone, filling anastomosing vugs between the grains, LT3, well Bsz-3 887.5 m, Zánka Sandstone, cross-polarized light (XPL). (b) Rhombic dolomite (dol3) precipitated in pore space among quartz grains (qz), and additionally anhydrite (anh) occurs, well Bsz-3 930 m, Zánka Sandstone, XPL. (c) Vug pores in LT1A, Bsz-3, 879.0 m, Csopak Fm., PPL. (d) Same as in c, exhibiting gypsum (gp) and anhydrite (anh) filling the vug pore, XPL.

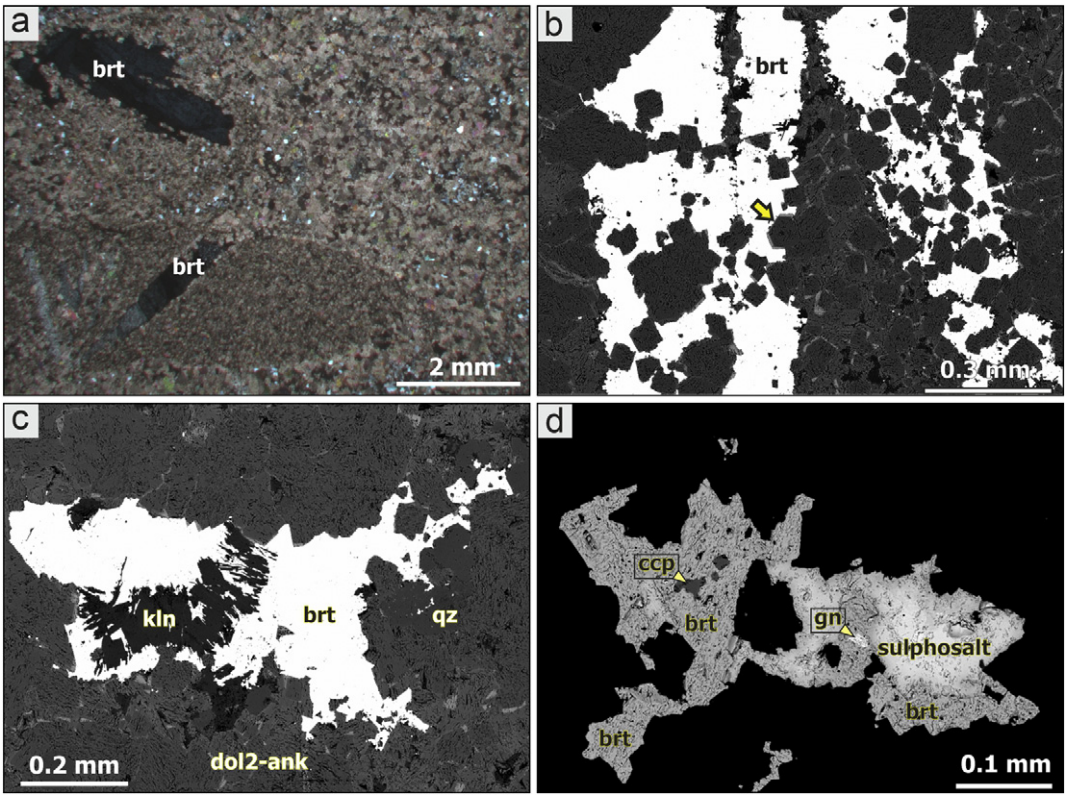

Fig. 12. Photomicrograph and backscattered-electron (BSE) images of barite (brt) occurring in LT2, well Kk-9, 294.8 m, Arács Fm. (a) Lath-shaped crystals (brt) in silty carbonate, cross-polarized light (XPL). (b) Barite (brt), enclosing zoned and corroded (arrow) dolomite (dol2) crystals, BSE image. (c) Barite (brt) intergrown with kaolinite filling a secondary pore in dolomite, BSE image. (d) Barite (brt) and sulphosalt filling a secondary pore in silty carbonate, enclosing remnants of chalcopyrite (ccp) and galena (gn), BSE image.

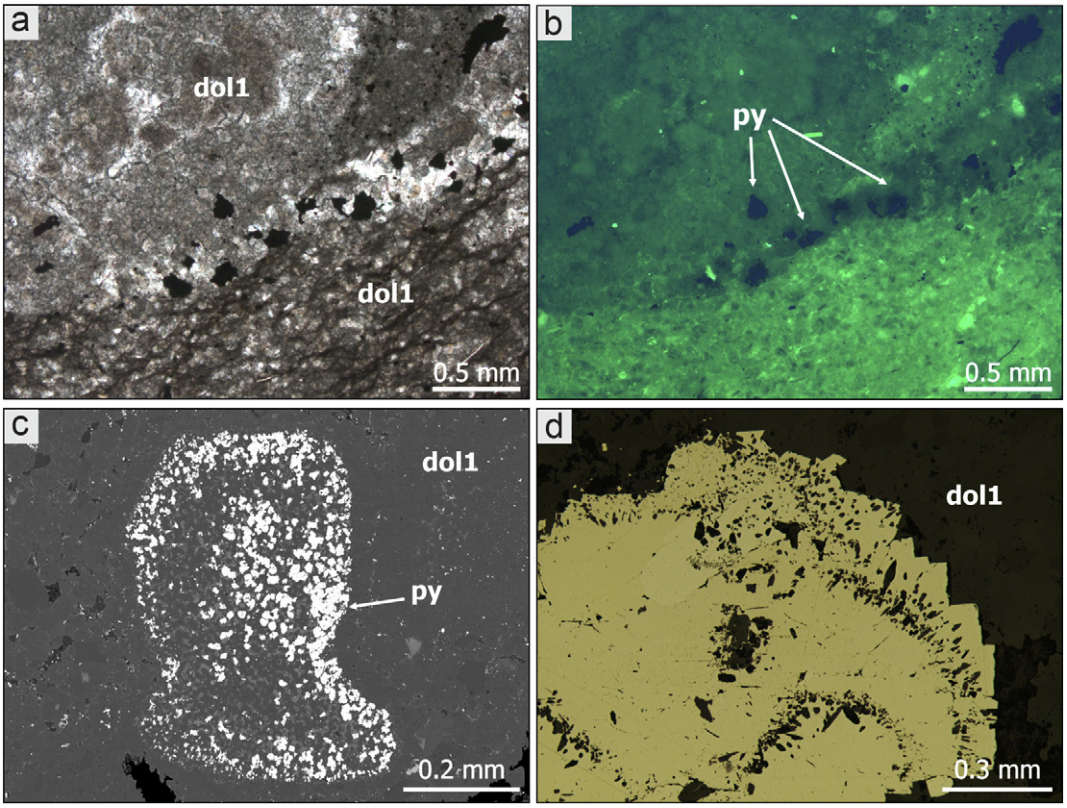

Fig. 13. Photomicrographs and backscattered-electron (BSE) image of sulphides in samples from LT2, well Kk-9, 294.8 m, Arács Fm. (a) Pyrite crystals along the boundary of organic-matter-rich and poor layers of dolomite, plane-polarized light (PPL). (b) Same as in "a" in blue light excitation. The dolomite in the lower part of the image is brownish and more fluorescent indicating higher organic matter content (c) Pyrite crystals in micropores of an echinoderm fragment, BSE image. (d) Pyrite with lens-shaped dolomite inclusions, reflected light. (For interpretation of the references to colour in this figure legend, the reader is referred to the web version of this article.)

sulphosalts seem to be coeval, the fluid at the time of precipitation should have been reducing. The barium was probably derived from diagenetic breakdown of K-feldspar and/or muscovite (Pe-Piper et al., 2015), which are present both in LT2,3 and the underlying Permian red sandstone (Budai et al., 1999). In the presence of sulfur, this process leads to immediate precipitation of barite. As lath-shaped barite can be a replacement of fibrous gypsum (Fig. 10b vs Fig. 12a) it is likely that the sulfur in the form of sulphate was in place and the barium was transported to the place of precipitation. Barite concretions were found in the Permian red sandstone, too (Balogh-Kiss and Molnár,

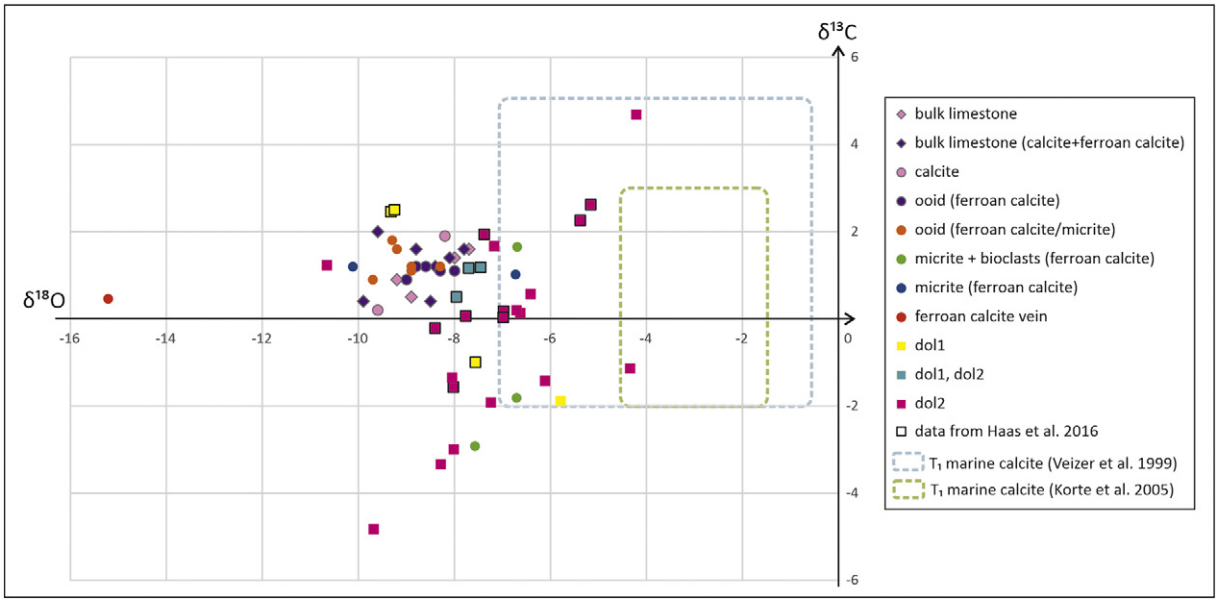

Fig. 14. Stable carbon and oxygen isotope compositions (in ‰ relative to V-PDB). Relationship between $\delta^{13}C$ and $\delta^{18}O$ values of dol1, dol2 phases, bulk limestone (LT5), calcitic components (micrite, bioclasts), ferroan calcite replacing ooids and fracture-filling ferroan calcite. Data of bulk limestone and calcitic components are from Hips and Haas (2009), whereas dolomite data marked by bold black outline are from Haas et al. (2017). (Data for calcite precipitated in equilibrium with Early Triassic seawater are from Veizer et al., 1999; Korte et al., 2005).

Diagenetic event			Diagenetic environment			
Process	Litho-type	Mineral phase	Eogenesis		Mesogenesis	Telogenesis
			Near-surface	Shallow burial	Intermediate to deep burial	Late near-surface
Formation of micritic envelope around bioclasts and ooids	1-2?,4,5		—			
Dissolution of aragonite	1-2?,4,5		—			
Precipitation of calcite in the biomolds and oomolds	1-2?,4,5		—			
Synsedimentary precipitation of evaporites	1	gp	—	—		
Synsedimentary and reflux dolomitization	1,2,3	dol1	—	—		
Compaction (Pressure dissolution + fracturing of quartz grains)	3			—		
Quartz cementation (fracture fill in quartz grains)	3	qz1		—	—	
Quartz cementation (overgrowth on quartz grains)	3	qz2		—	—	
Hydrothermal dolomitization	1-4	dol2-3,ank			—	
Gypsum dewatering to form anyhdrite	1,2,3	anh			—	
Kaolinite	1,2	kln			—	
Galenite	1,2	gn			—	
Chalcopyrite	1,2	ccp			—	
Pyrite	1,2	py			—	
Barite	1,2	brt			—	
Sulphosalt	1,2				—	
Ferroan calcite replacing dolomite	4,5					—
Fracture-filling ferroan calcite	1,4,5					—
Anyhdrite hydration to form gypsum	1,2,3	gp				—

Fig. 15. Paragenetic sequence of minerals and diagenetic events for the different lithotypes. (Abbreviations: gp – gypsum, dol – dolomite, qz – quartz, anh – anhydrite, kln – kaolinite, gn – galena, ccp – chalcopyrite, py – pyrite, brt – barite).

2014), suggesting that the process was active already in the underlying beds. The barium-rich fluid most probably transported metals. Metal oxides and hydroxides of the underlying red sandstone; and organic matter, K-feldspar in interbedded sandstone, carbonate phases or shales could be the source of As, Sb, Cu, Pb and Zn (Sverjensky, 1984, 1987; Kharaka et al., 1987; Hanor, 1996).

Brines are the most efficient transporters of metals in the form of chloride complexes (e.g., Hanor, 1996). To transport metals, a brine salinity higher than 10% NaCl equivalent is required. However, salinities as high as 17% are more efficient (Giordano, 2002). The metal transportation is more effective at elevated temperatures (Yardley, 2005). The results of chemical reaction path modellings show that the highest metal content occurs in fluids of low pH, low content of reduced sulfur, and high chloride content (Leach et al., 1991). These types of solutions faciliate the transport of significant amount of base metals (ppm of Pb and Zn) with reduced sulfur. High CO_2 content favours the precipitation of dolomite, kaolinite and sulphide, whereas the locally high H_2S content lead to formation of only limited amounts of sulphides. Low-salinity fluids precipitate less sulphide and more dolomite, and the contrary happens when the fluid has elevated temperature.

Since chloride-rich minerals are not known from the underlying strata, it is more probable that the metals were transported in carboxylate complexes (cf., Giordano, 2000). Carboxylate ligands present in petroleum-related brines are also capable of complexing Ca, Mg, Fe and Al (Giordano, 2002). This complexing, however, is rare and could not account for transportation of significant metal amounts. The lack of larger mineralization can be explained by the limited supply of metal-transporting fluids, the limited availability of metals, or, alternatively, the availability of sulfur. The lack of sulphate minerals in the ore-rich strata seems to support the latter option. The precipitation of metals could have happened due to (1) temperature and/or pressure decrease in the upward migrating fluids, (2) mixing of the fluids with the evolved pore water of the Lower Triassic beds, or (3) fluid/rock interaction causing pH and Eh shifts (cf., Ramboz et al., 1982; Robb, 2004; Chi and Xu, 2011).

5.5. Calcitization of dolomite (dedolomitization)

The serrated boundaries between calcite/ferroan calcite and ferroan dolomite-ankerite (dol2-ank) within LT4 (Fig. 8e) along with the curved crystal planes and undulose extinction of the calcite/ferroan calcite phases in LT5 (Fig. 9c) indicate that the calcite is a replacement of dolomite (Fig. 15d). The presence of dolomite inclusions within the calcite also suggest that the dolomite phase preceded the calcite. Some of the coarse, ferroan calcite crystals within spheroidal grains in LT5 still contain tiny dolomite inclusions. The lower $\delta^{18}O$ values of the ferroan calcite samples suggest higher temperature than that of the dolomitizing fluid (dol2-ank and dol3).

6. Conclusions

The Lower Triassic peritidal-shallow marine, mixed siliciclastic-carbonate succession of the Transdanubian Range was subdivided into five lithotypes, from dolomite through sandstone/siltstone to limestone, displaying different degree of dolomitization and different amount of siliciclastics.

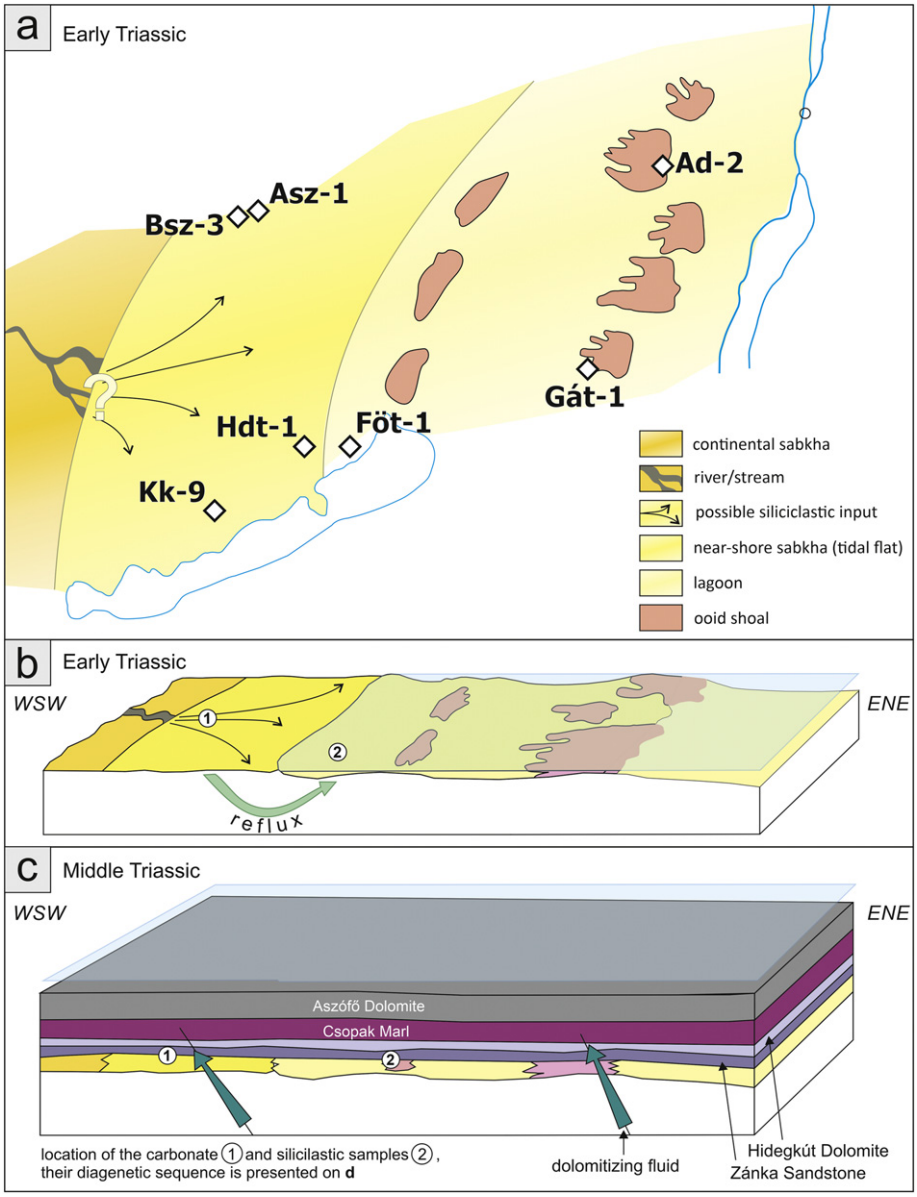

Fig. 16. (a) Paleoenvironmental map of the Transdanubian Range during the Early Triassic (b) Arrangement of the environments in SW-NE cross section during Early Triassic, (c) Arrangement of the environments in SW-NE cross-section during the Middle Triassic. Green arrows show the migration pathway of the dolomitizing fluids. (d) Schematic model for the dolomitization and other diagenetic processes that affected the Lower Triassic mixed lithotypes. (1) Diagenetic events in the dolomite, dolomitic limestone and limestone lithotypes (LT1, LT4, LT5). (2) Diagenetic events in the sandstone lithotype (LT3) These numbers correspond to those on figures (b) and (c). (For interpretation of the references to colour in this figure legend, the reader is referred to the web version of this article.)

The most important findings of the study:

1. Shallow marine, reflux dolomitization affected the carbonate-rich lithotypes, deposited closer to shoreface and rich in sulphate minerals, whereas ooid shoal deposits were partially dolomitized.
2. Iron and manganese were released from the clay minerals during medium to deep burial in the siliciclastic rocks and were incorporated into dolomite and ankerite replacive and cement phases. This ferroan dolomite and ankerite phases also appear in the previously completely or partially dolomitized lithotypes. Stable isotope and petrographic data of the dolomite phases indicate that the first dolomitization event was overprinted by this higher temperature event, which involved the flux of dolomitizing fluids. These fluids replaced the former dolomite phases and precipitated as cement regardless of the host rock.
3. The barite-sulphide mineral association, in the dolomite and in the silty and sandy dolomite-dolomarl lithotypes, suggests that the high-temperature dolomitizing fluid, which ascended along faults from the underlying Permian evaporites and red sandstone beds, transported metals, too. The fluids reacted with the wall rocks, became acidic and reducing that resulted in: (i) dissolution and transport of Fe and other cations such as Sb, As, Cu, Zn, Hg, most probably from the underlying red sandstone, (ii) formation of vugs of the Lower Triassic limestone/dolomite, and (iii) replacement of the gypsum by barite.

The results imply that even in mixed shallow-water sediments excessive dolomitization can be attributed to reflux processes. Smaller scale dolomitization events can benefit from the vicinity of (especially organic-rich) siliciclastic strata, as they contain the necessary minerals that can provide Mg (e.g., clay minerals), and even Fe and Mn that can be incorporated into different ferroan carbonate phases. On the other hand, such process can mostly be effective if these fluids are transported

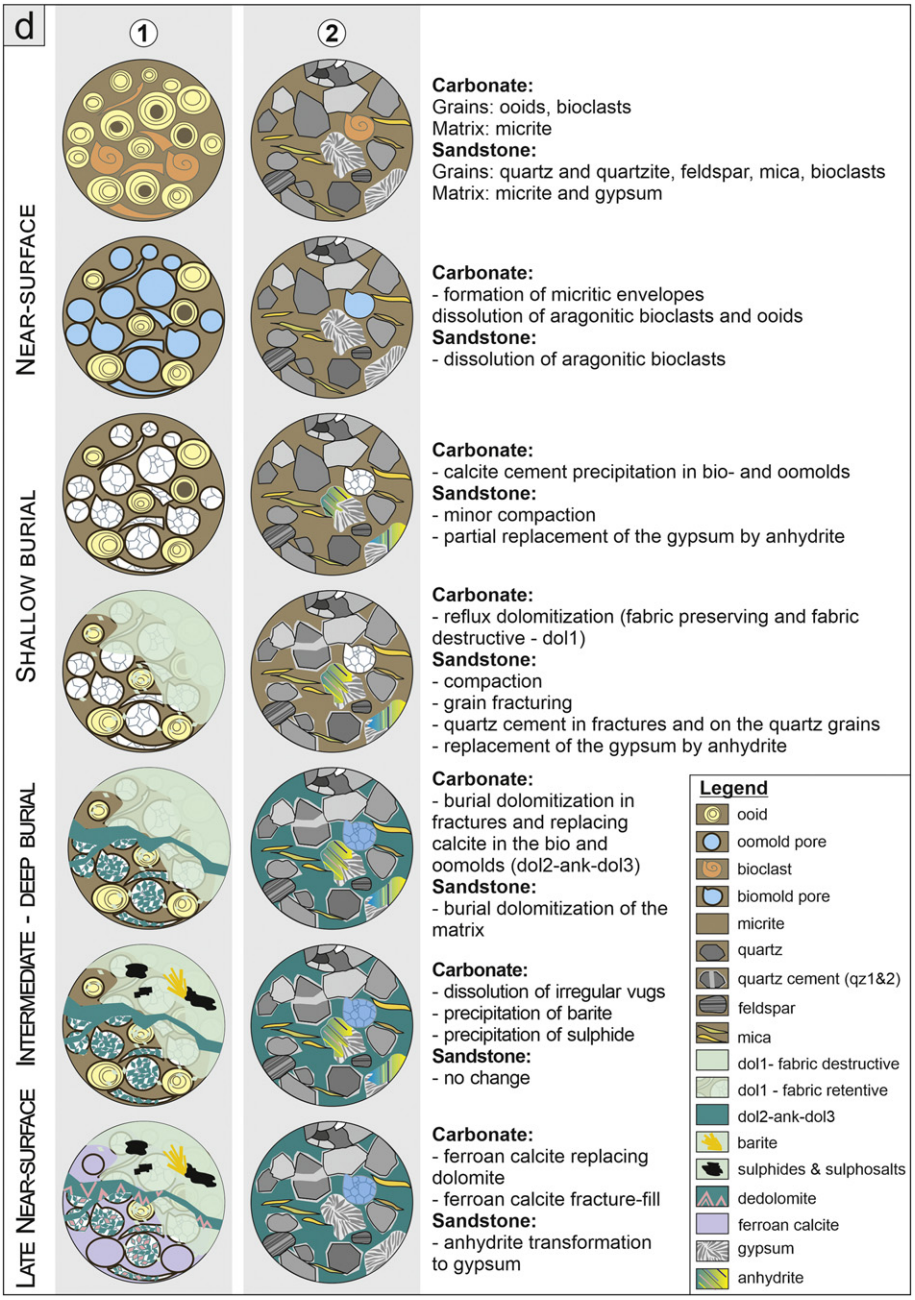

Fig. 16 (*continued*).

through fractures. Therefore, it is more likely to be associated with local to regional tectonic events.

Declaration of competing interest

The authors declare that they have no known competing financial interests or personal relationships that could have appeared to influence the work reported in this paper.

Acknowledgements

The Mining and Geological Survey of Hungary kindly provided thin sections and wellbook information of the studied cores and wells. Comments of Jasper Knight, Sadoon Morad, Roman Aubrecht and an anonymous reviewer improved the manuscript and are highly appreciated. The help of István Hegyi during the stable isotope measurements is acknowledged. We are thankful to Ádám Kovács, Aurelien Meyer, Zsófia Poros and Ágnes Török for discussions on the topic. This work was supported by the Hungarian Scientific Research Fund (OTKA K124313).

Appendix A. Supplementary data

Supplementary data to this article can be found online at https://doi.org/10.1016/j.sedgeo.2019.105549.

References

Al-Helal, A.B., Whitaker, F.F., Xiao, Y., 2012. Reactive transport modeling of brine reflux: Dolomitization, anhydrite precipitation, and porosity evolution. J. Sediment. Res. 82, 196–215.

Anderson, T.F., Arthur, M.A., 1983. Stable isotopes of oxygen and carbon and their application to sedimentologic and paleoenvironmental problems. In: Arthur, M.A. (Ed.), Stable Isotopes in Sedimentary Geology. SEPM Short Course 10. Section 1, 19–1.151.

Anjos, S.M.C., De Ros, L.F., Souza, R.S., Silva, C.M.A., Sombra, C.L., 2000. Depositional and diagenetic controls on the reservoir quality of Lower Cretaceous Pendência sandstones, Potiguar rift basin. Brazil. AAPG Bulletin 84, 1719–1742.

Balogh-Kiss G., Molnár, F., 2014. A Balatonfelvidéki Homokkőben található geódák ásványtani és genetikai vizsgálata. Mineralogical and genetic study of geodes from the Balatonfelvidék Sandstone Formation (in Hungarian). In: Fehér, B. (Ed.), Az ásványok vonzásában. Miskolc, 15–26.

Bassant, P., Janson, X., Buchem, F., Gurbuz, K., Eris, K., 2017. Mut Basin, Turkey: Miocene carbonate depositional styles and mixed systems in an icehouse setting. AAPG Bull. 101, 533–541.

Blanchard, S., Fielding, C.R., Frank, T.D., Barrick, J.E., 2016. Sequence stratigraphic framework for mixed aeolian, peritidal and marine environments: insights from the Pennsylvanian subtropical record of Western Pangaea. Sedimentology 63, 1929–1970.

Blomme, K., Fowler, S.J., Swennen, R., Nader, F.H., Bachaud, P., 2015. Quantitative testing of conceptual models for hydrothermal carbonate genesis: the Latemar platform. Bathurst Conference 2015, Abstract Book, 33.

Boles, J.R., 1977. Active ankerite cementation in the subsurface Eocene of Southwest Texas. Contrib. Mineral. Petrol. 68, 13–22.

Boles, J.R., Franks, S.G., 1979. Clay diagenesis in Wilcox Sandstones of Southwest Texas: Implications of smectite diagenesis on sandstone cementation. J. Sediment. Petrol. 49, 55–70.

Broglio Loriga, C., Góczán, F., Haas, J., Lenner, K., Tóth-Makk, Á., 1990. The Lower Triassic sequences of the Dolomites (Italy) and Transdanubian Mid-Mountains (Hungary) and their correlation. Memorie di Scienze Geologiche 42, 41–103.

Budai, T., Haas, J., 1997. Triassic sequence stratigraphy of the Balaton Highland (Hungary). Acta Geol. Hung. 40, 307–335.

Budai, T., Császár, G., Csillag, G., Dudko, A., Koloszár, L., Majoros, Gy, 1999. Geology of the Balaton Highland. Hungarian Geological Institute, Budapest.

Canet, C., Anadón, P., Alfonso, P., Prol-Ledesma, R.M., Villanueva-Estrada, R.E., García-Vallčs, M., 2013. Gas-seep related carbonate and barite authigenic mineralization in the northern Gulf of California. Mar. Pet. Geol. 43, 147–165.

Caracciolo, L., Gramigna, P., Critelli, S., Calzona, A.B., Russo, F., 2013. Petrostratigraphic analysis of a Late Miocene mixed siliciclastic–carbonate depositional system (Calabria, Southern Italy): Implications for Mediterranean paleogeography. Sediment. Geol. 284–285, 117–132.

Carrol, D., 1958. Role of clay minerals in the transportation of iron. Geochim. Cosmochim. Acta 14, 1–28.

Chi, G., Xu, C., 2011. An overview of hydrodynamic studies of mineralization. Geosci. Front. 1, 423–438.

Chiarella, D., Longhitano, S.G., Tropeano, M., 2017. Types of mixing and heterogeneities in siliciclastic-carbonate sediments. Mar. Pet. Geol. 88, 617–627.

Coffey, B.P., Read, F., 2007. Subtropical to temperate facies from a transition zone, mixed carbonate–siliciclastic system, Palaeogene, North Carolina, USA. Sedimentology 54, 339–365.

Coffey, B.P., Sunde, R., 2014. Lithology-based sequence-stratigraphic framework of a mixed carbonate-siliciclastic succession, Lower Cretaceous, Atlantic coastal plain. AAPG Bull. 98, 1599–1630.

Coplen, T.B., Hanshaw, B.B., 1973. Ultrafiltration by a compacted clay membrane: I. Oxygen and hydrogen isotopic fractionation. Geochimica et Cosmochimica Acta 37, 2295–2310.

Csalagovits, I., Virágh, K., 1968. Rétegtani szinthez kötött réz és ólom-cink indikációk a Magyar Népköztársaság területén. I–II Sedimentary copper-lead ore indications in Hungary. (in Hungarian). Report of the Hungarian Geological Institute. Budapest. 74 Manuscript.

Császár, G., Haas, J., 1979. Review of the facies and palaeogeography of the Cretaceous in Hungary. In: Wiedmann, J. (Ed.), Aspekte der Kreide Europas. vol. 6, pp. 413–424 IUGS Series, A 6: 1–9 Stuttgart, Schweizerbart.

Csontos, L., Vörös, A., 2004. Mesozoic plate tectonic reconstruction of the Carpathian region. Palaeogeogr. Palaeoclimatol. Palaeoecol. 210, 1–56.

Csontos, L., Nagymarosy, A., Horváth, F., Kovác, M., 1992. Cenozoic evolution of the Intra-Carpathian area: a model. Tectonophysics 208, 221–241.

Danisik, M., Fodor, L., Dunkl, I., Gerdes, A., Csizmeg, J., Hámor-Vidó, M., Evans, N.J., 2015. A multi-system geochronology in the Ad-3 borehole, Pannonian Basin (Hungary) with implications for dating volcanic rocks by low-temperature thermochronology and for interpretation of (U–Th)/He data. Terra Nova 27, 258–269.

Dickson, J.A.D., 1966. Carbonate identification and genesis as revealed by staining. J. Sediment. Res. 36, 491–505.

Elias, A.R.D., De Ros, L.F., Mizusaki, A.M.P., Kawashita, K., 2007. Isotopic evidence on the diagenetic evolution of coastal sabkha reservoirs from the Solimões Basin. northern Brazil. Gondwana Research 11, 553–567.

Fodor, L., 1998. Late Mesozoic and Early Paleogene tectonics of the Transdanubian Range. XIVth CBGA Congress Vienna, Austria, Geological Survey of Austria 165.

Folk, R.L., 1962. Spectral subdivision of limestone types. In: Ham, W.E. (Ed.), Classification of Carbonate Rocks — A Symposium. vol. 1, pp. 62–84 Tulsa, OK, AAPG Memoir.

Fritz, P., Smith, D.G.W., 1970. The isotopic composition of secondary dolomites. Geochim. Cosmochim. Acta 34, 1161–1173.

Gabellone, T., Whitaker, F., 2016. Secular variations in seawater chemistry controlling dolomitisation in shallow reflux systems: insights from reactive transport modelling. Sedimentology 63, 1233–1259.

Giordano, T.H., 2000. Organic matter as transport agent in ore-forming systems. Rev. Econ. Geol. 9, 133–156.

Giordano, T.H., 2002. Transport of Pb and Zn by carboxylate complexes in basinal ore fluids and related petroleum-field brines at 100 °C: the influence of pH and oxygen fugacity. Geochem. Trans. 3, 56–72.

Góczán, F., Oravecz-Scheffer, A., Szabó, I., 1986. Biostratigraphic zonation of the Lower Triassic in the Transdanubian Central Range. Acta Geol. Hung. 29, 233–259.

Gregg, J.M., 1988. Origins of dolomite in the offshore facies of the Bonneterre Formation (Cambrian), Southeast Missouri. In: Shukla, V., Baker, P.A. (Eds.), Sedimentology and Geochemistry of Dolostones. vol. 43, pp. 67–83 Society for Sedimentary Geology Special Publication.

Haas, J., Budai, T., 1995. Upper Permian–Triassic facies zones in the Transdanubian Range. Rivista Italiana Paleontologia Stratigrafia 101, 249–266.

Haas, J., Budai, T., 1999. Triassic sequence stratigraphy of the Transdanubian Range (Hungary). Geol. Carpath. 50, 459–475.

Haas, J., Tóth-Makk, Á., Oravecz-Scheffer, A., Góczán, F., Oravecz, J., Szabó, I., Vető, I., Kubovics, I., Szabó, Cs, 1988. Lower Triassic key sections in the Transdanubian Mid-Mountains. Annales of the Hungarian Geological Institute 65 (356 pp).

Haas, J., Kovács, S., Krysyin, L., Lein, R., 1995. Significance of Late Permian-Triassic facies zones in terrane reconstructions in the Alpine-North Pannonian domain. Tectonophysics 242, 19–40.

Haas, J., Budai, T., Raucsik, B., 2012. Climatic controls on sedimentary environments in the Triassic of the Transdanubian Range (Western Hungary). Palaeogeogr. Palaeoclimatol. Palaeoecol. 353–355, 31–44.

Haas, J., Hips, K., Budai, T., Győri, O., Lukoczki, G., Kele, S., Demény, A., Poros, Zs., 2017. Processes and controlling factors of polygenetic dolomite formation in the Transdanubian Range, Hungary: a synopsis. Int. J. Earth Sci. 106, 991–1021.

Haas, J., Budai, T., Hips, K., Kriványné, H.Á. (Eds.), 2004: Magyarország geológiája – Triász. Geology of Hungary - Triassic (in Hungarian). ELTE Eötvös Kiadó, (384 pp).

Hanor, J.S., 1996. Controls on the solubilization of lead and zinc in basinal brines. In: Sangster, D.F. (Ed.), Carbonate-Hosted Lead-Zinc Deposits. vol. 4, pp. 483–500 Society for Sedimentary Geology Special Publication.

Hendry, J.P., Wilkinson, M., Fallick, A.E., Haszeldine, R.S., 2000a. Ankerite cementation in deeply buried Jurassic sandstones reservoirs of the Central North Sea. J. Sediment. Res. 70, 227–239.

Hendry, J.P., Wilkinson, M., Fallick, A.E., Haszeldine, R.S., 2000b. Ankerite cementation in deeply buried Jurassic sandstone reservoirs of the Central North Sea. J. Sediment. Res. 70, 227–239.

Hips, K., Haas, J., 2009. Facies and diagenetic evaluation of the Permian-Triassic boundary interval and basal Triassic carbonates: shallow and deep ramp sections, Hungary. Facies 55, 421–442.

Hower, J., Eslinger, E.V., Hower, M.E., Perry, E.A., 1976. Mechanism of burial metamorphism of argillaceous sediment: 1. Mineralogical and chemical evidence. GSA Bull. 87, 725–737.

Imam, M.B., Shaw, H.F., 1985. The diagenesis of Neogene clastic sediments from the Bengal Basin. J. Sediment. Petrol. 55, 665–671.

Irwin, H., Curtis, C., Coleman, M., 1977. Isotopic evidence during burial of organic-rich sediments. Nature 269, 209–213.

Johnes, G.D., Xiao, Y., 2005. Dolomitization, anhydrite cementation, and porosity evolution in a reflux system: Insights from reactive transport models. AAPG Bull. 89, 577–601.

Kantorowicz, J.D., 1985. The origin of authigenic ankerite from the Ninian Field, UK North Sea. Nature 315, 214–216.

Kázmér, M., Kovács, S., 1985. Permian–Paleogene paleogeography along the Eastern part of the Insubric–Periadriatic Lineament system: evidence for continental escape of the Bakony–Drauzug Unit. Acta Geol. Hung. 28, 71–84.

Khalifa, M.A., Mansurbeg, H., Morad, D., Morad, S., Al-Aasm, I.S., Spirov, P., De Ros, L.F., 2018. Quartz and Fe-dolomite cements record shifts in formation-water chemistry and hydrocarbon migration in Devonian shoreface sandstones, Ghadamis Basin. Libya. Journal of Sedimentary Research 88, 38–57.

Kharaka, Y.K., Maest, A.S., Carothers, W.W., Law, L.M., Lamothe, P.J., Fried, T.L., 1987. Geochemistry of metal-rich brines from Central Mississippi Salt Dome Basin. USA. Applied Geochemistry 2, 543–561.

Kleipool, L.M., Reijmer, J.J.G., Badenas, B., Aurell, M., 2015. Variations in petrophysical properties along a mixed siliciclastic carbonate ramp (Upper Jurassic, Ricla, NE Spain). Mar. Pet. Geol. 68, 158–177.

Korngreen, D., Bialik, O.M., 2015. The characteristics of carbonate system recovery during a relatively dry event in a mixed carbonate/siliciclastic environment in the Pelsonian (Middle Triassic) proximal marginal marine basins: a case study from the tropical Tethyan Northwest Gondwana margins. Palaeogeogr. Palaeoclimatol. Palaeoecol. 440, 793–812.

Korte, C., Kozur, H., Veizer, J., 2005. $\delta^{13}C$ and $\delta^{18}O$ values of Triassic brachiopods and carbonate rocks as proxies for coeval seawater and palaeotemperature. Palaeogeogr. Palaeoclimatol. Palaeoecol. 226, 287–306.

Land, L.S., 1980. The isotopic and trace element geochemistry of dolomite: the state of the art. In: Zenger, D.H., Dunham, J.B., Ethington, R.L. (Eds.), Concepts and Models of Dolomitization. vol. 28, pp. 87–110 Society for Sedimentary Geology Special Publication.

Leach, D.L., Plumlee, G.S., Hofstra, A.H., Landis, G.P., Rowan, E.L., Viets, J.G., 1991. Origin of late dolomite cement by CO_2-saturated deep basin brines: evidence from the Ozark region, Central United States. Geology 19, 348–351.

Macaulay, C.I., Haszeldine, R.S., Fallick, A.E., 1993. Distribution, chemistry, isotopic composition and origin of diagenetic carbonates: Magnus Sandstone. North Sea. Journal of Sedimentary Petrology 63, 33–43.

Machel, H., 2004. Concepts and models of dolomitization: a critical reappraisal. In: Braithwaite, C.J.R., Rizzi, G., Darke, G. (Eds.), The Geometry and Petrogenesis of Dolomite Hydrocarbon Reservoirs. vol. 235, pp. 7–63 Geological Society, London, Special Publications.

Machel, H., Krouse, H.R., Sassen, R., 1995. Products and distinguishing criteria of bacterial and thermochemical sulfate reduction. Appl. Geochem. 10, 373–389.

Majoros, Gy, 1998. A Dunántúli-középhegység újpaleozoos képződményeinek rétegtana. Stratigraphy of the Paleosoic strata in the Transdanubian Range (in Hungarian). In: Bérczi, I., Jámbor, Á. (Eds.), Magyarország geológiai képződményeinek rétegtana. Budapest, MOL and Geological Institute of Hungary, pp. 119–148.
Márton, E., Márton, P., 1996. Large scale rotations in North Hungary during the Neogene as indicated by palaeomagnetic data. In: Morris, A, Tarling, D.H. (Eds.), PAleomagnetism and Tectonics of the Mediterranean Region. Geological Society, London, Special Publications vol. 105, pp. 153–173.
McBride, E.F., 1989. Quartz cement in sandstones: a review. Earth-Sci. Rev. 26, 69–112.
McHargue, T.R., Price, R.C., 1982. Dolomite from clay in argillaceous or shale-associated marine carbonates. J. Sediment. Petrol. 52, 873–886.
McNeill, D.F., Cunningham, K.J., Guertin, L.A., Anselmetti, F.S., 2004. Depositional themes of mixed carbonate-siliciclastics in the South Florida Neogene: application to ancient deposits. In: Grammer, G.M. (Ed.), Integration of Outcrop and Modern Analogs in Reservoir Modeling. vol. 80, pp. 23–43 AAPG Memoir.
Meunier, A., 2005. Clays. Springer-Verlag, Berlin, Germany.
Milliken, K.L., 2003. Late diagenesis and mass transfer in sandstone–shale sequences. In: Mackenzie, F. (Ed.), Treatise on Geochemistry 7: Sediments, Diagenesis, and Sedimentary Rocks. Elsevier, Amsterdam, The Netherlands, pp. 159–190.
Mindszenty, A., 1985. The lithology of some Hungarian bauxites - a contribution to the palaeogeographic reconstruction. Acta Geol. Hung. 27, 441–455.
Moore, C.H., 1997. Carbonate Diagenesis and Porosity. Developments in Sedimentology, Elsevier, Amsterdam, The Netherlands.
Morad, S., 1998. Carbonate Cementation in Sandstones. Special Publication 26 of the IAS. Great Britain, Blackwell Science, Cambridge.
Morad, S., De Ros, L.F., 1994. Geochemistry and diagenesis of stratabound calcite cement layers within the Rannoch Formation of the Brent Group, Murchison Field, North Viking Graben (northern North Sea). Sediment. Geol. 93, 135–141.
Morad, S., Ketzer, J.M., De Ros, F., 2000. Spatial and temporal distribution of diagenetic alterations in siliciclastic rocks: implications for mass transfer in sedimentary basins. Sedimentology 47, 95–120.
Morad, S., Al-Aasm, I.S., Nader, F.H., Ceriani, A., Gasparrini, M., Mansurbeg, H., 2012. Impact of diagenesis on the spatial and temporal distribution of reservoir quality in the Jurassic Arab D and C members, offshore Abu Dhabi oilfield, United Arab Emirates. GeoArabia 17, 17–56.
Oldershaw, A.E., Scoffin, T.P., 1967. The source of ferroan and non-ferroan calcite cements in the Halkin and Wenlock limestones. Geol. J. 5, 309–320.
Pe-Piper, G., Piper, D.J.W., Zhang, Y., Chavez, I., 2015. Diagenetic barite and sphalerite in middle Mesozoic sandstones, Scotian Basin, as tracers for basin hydrology. AAPG Bull. 99, 1281–1313.
Pye, K., 1985. Electron microscope analysis of zoned dolomite rhombs in the Jet Rock Formation Lower Toarcian of the Whitby area UK. Geol. Mag. 122, 279–286.
Pye, K., Krinsley, D.H., 1986. Diagenetic carbonate and evaporite minerals in Rotliegend aeolian sandstones of the southern North Sea: their nature and relationship to secondary porosity development. Clay Miner. 21, 443–457.
Raincsák, Gy., 1975. Színesérc indikációk a Veszprém környéki werfeni rétegekben. (Ore indication in the Werfen beds around Veszprém (in Hungarian). Yearly Report of the Geological Insititue of Hungary about 1975, 249–253.
Raincsák, Gy., 1982. Alsó-triász sztratiform ércképződés lehetőségének vizsgálata Veszprém-Litér-Sóly között és az Iszka-hegy környékén. (Ore indications in the Werfen beds near Veszprém (in Hungarian). Yearly Report of the Geological Insititue of Hungary about 1982, 245–260.
Ramboz, C., Pichavant, M., Weisbrod, A., 1982. Fluid immiscibility in natural processes: use and misuse of fluid inclusion data II. Interpretation of fluid inclusion data in terms of immiscibility. Chem. Geol. 37, 29–48.
Reis, H.L.S., Suss, J.F., 2016. Mixed carbonate–siliciclastic sedimentation in forebulge grabens: an example from the Ediacaran Bambuí Group, São Francisco Basin, Brazil. Sediment. Geol. 339, 83–103.
Richter, D.K., Fuchtbauer, H., 1978. Ferroan calcite replacement indicates former magnesian calcite skeletons. Sedimentology 25, 843–860.
Robb, L., 2004. Introduction to Ore-Forming Processes. Wiley-Blackwell, Cambridge, Great Britain.
Rosenbaum, J., Sheppard, S.M.F., 1986. An isotopic study of siderites, dolomites and ankerites at high temperatures. Geochimica et Cosmochemica Acta 50, 1147–1150.
Saller, A.H., Henderson, N., 1998. Distribution of porosity and permeability in platform dolomites: Insight from the Permian of West Texas. AAPG Bull. 82, 1528–1550.
Schmid, S., 2004. Diagenesis and reservoir quality of the Sherwood Sandstone (Triassic), Corrib Field, Slyne Basin, west of Ireland. Mar. Pet. Geol. 21, 299–315.
Schmid, S.M., Bernoulli, D., Fügenschuch, B., Matenco, L., Schefer, S., Schuster, R., Tischler, M., Ustaszewski, K., 2008. The Alpine–Carpathian–Dinaridic orogenic system: correlation and evolution of tectonic units. Swiss J. Geosci. 101, 139–183.
Sheppard, S.M.F., Schwarcz, H.P., 1970. Fractionation of carbon and oxygen isotopes and magnesium between coexisting metamorphic calcite and dolomite. Contrib. Mineral. Petrol. 26, 161–198.
Smith, J.T., Ehrenberg, S.N., 1989. Correlation of carbon dioxide abundance with temperature in clastic hydrocarbon reservoirs: relationship to inorganic chemical equilibrium. Mar. Pet. Geol. 6, 129–135.
Souza, R.S., De Ros, L.F., Morad, S., 1995. Dolomite diagenesis and porosity preservation in lithic reservoirs: Carmópolis Member, Sergipe-Alagoas Basin. northeastern Brazil. AAPG Bulletin 79, 725–748.
Spötl, C., Vennemann, T.W., 2003. Continuous-flow isotope ratio mass spectrometric analysis of carbonate minerals. Rapid Commun. Mass Spectrom. 17, 1004–1006.
Sullivan, M.D., Haszeldine, R.S., Fallick, A.E., 1990. Linear coupling of carbon and strontium isotopes in Rotliegend Sandstone, North Sea: evidence for cross-formational fluid flow. Geology 18, 1215–1218.
Sverjensky, D.A., 1984. Oil field brines as ore-forming solutions. Econ. Geol. 79, 23–37.
Sverjensky, D.A., 1987. The role of migrating oil field brines in the formation of sediment – hosted Cu-rich deposits. Econ. Geol. 82, 1130–1141.
Taylor, T.R., Sibley, D.F., 1986. Petrographic and geochemical characteristics of dolomite types and the origin of ferroan dolomite in the Trenton Formation Ordovician Michigan Basin. Sedimentology 33, 61–86.
Tucker, M.E., Wright, V.P., 1990. Carbonate Sedimentology. Blackwell Science Ltd, Cambridge, Great Britain.
Veizer, J., Ala, D., Azmy, K., Bruckschen, P., Buhl, D., Bruhn, F., Carden, G.A.F., Diener, A., Ebneth, S., Godderis, Y., Jasper, T., Korte, C., Pawellek, F., Podlaha, O.G., Strauss, H., 1999. $^{87}Sr/^{86}Sr$, $\delta^{13}C$ and $\delta^{18}O$ evolution of Phanerozoic seawater. Chem. Geol. 161, 59–88.
Yardley, B.W.D., 2005. Metal concentrations in crustal fluids and their relationship to ore formation. Econ. Geol. Bull. Soc. Econ. Geol. 100, 613–632.
Zeller, M., Verwe, K., Eberli, G.P., Massaferro, J.L., Schwarz, E., Spalletti, L., 2015. Depositional controls on mixed carbonate–siliciclastic cycles and sequences on gently inclined shelf profiles. Sedimentology 62, 2009–2037.